AFAL-TR-78-31

LEVEL III 2

AD 59 085

HIGH DENSITY MAGNETIC BUBBLE MEMORY TECHNIQUES

Electronics Research Center
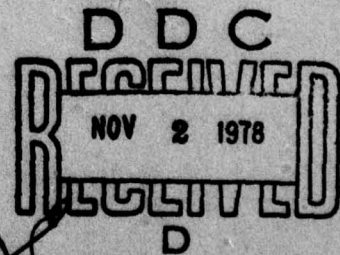Rockwell International
Anaheim, California

March 1978

Technical Report AFAL-TR-78-31

Interim Report for 4 May 1977 to 4 November 1977

Approved for public release; distribution unlimited

D D C
RECEIVED
NOV 2 1978
D

Air Force Avionics Laboratory
Air Force Wright Aeronautical Laboratories
Air Force Systems Command
Wright-Patterson AFB, Ohio 45433

78 10 27 027

DR. MILLARD G. MIER
Project Engineer

FOR THE COMMANDER

ROBERT D. LARSON, Chief
Electronic Research Branch
Electronic Technology Division

REPORT DOCUMENTATION PAGE	READ INSTRUCTIONS BEFORE COMPLETING FORM

1. REPORT NUMBER	2. GOVT ACCESSION NO.	3. RECIPIENT'S CATALOG NUMBER
AFAL-TR-78-31		

4. TITLE (and Subtitle)

HIGH DENSITY MAGNETIC BUBBLE MEMORY TECHNIQUES

5. TYPE OF REPORT & PERIOD COVERED

4 May 1977 to 4 November 1977 Interim

6. PERFORMING ORG. REPORT NUMBER

C76-845.16/501

7. AUTHOR(s)

P. J. Besser   T. Kobayashi
D. M. Heinz   T. T. Chen
        L. R. Tocci

8. CONTRACT OR GRANT NUMBER(s)

F33615-76-C-1198

9. PERFORMING ORGANIZATION NAME AND ADDRESS

Rockwell International
Electronics Research Center
Anaheim, California

10. PROGRAM ELEMENT, PROJECT, TASK AREA & WORK UNIT NUMBERS

2305 R2 61   R2

11. CONTROLLING OFFICE NAME AND ADDRESS

Air Force Avionics Laboratory, (DHR)
Wright-Patterson AFB, Ohio 45433   61102F

12. REPORT DATE

March 1978

13. NUMBER OF PAGES

57   61 p.

14. MONITORING AGENCY NAME & ADDRESS(if different from Controlling Office)

15. SECURITY CLASS (of this report)

Unclassified

15a. DECLASSIFICATION DOWNGRADING SCHEDULE

16. DISTRIBUTION STATEMENT (of this Report)

Approved for public release; distribution unlimited.

Interim rept. 4 May – 4 Nov 77.

17. DISTRIBUTION STATEMENT (of the abstract entered in Block 20, if different from Report)

18. SUPPLEMENTARY NOTES

19. KEY WORDS (Continue on reverse side if necessary and identify by block number)

High Capacity Chip Design
Multilayer Bubble Materials
Magnetic Bubble Devices
Self Biased Bubble Materials

20. ABSTRACT (Continue on reverse side if necessary and identify by block number)

In an effort to improve the temperature properties of self-biased films a number of films with biasing layers and capping layers were grown. The complexity of this material system prompted a study of the individual film properties first before the multiple layer films were evaluated. Bubble layer composition was principally $(YSm)_3(GaFe)_5O_{12}$, while the biasing layer and capping layers were $(ErEu)_3(GaFe)_5O_{12}$ (or $(ErEuCa)_3(GeFe)_5O_{12}$) and $(YLa)_3(GaFe)_5O_{12}$, respectively.

DD FORM 1473   EDITION OF 1 NOV 65 IS OBSOLETE

A number of resist techniques necessary to etch mesa's in the self-biased films for stability in the biasing layer were evaluated. The most promising approach thus far uses an organosilicon solution. The problem which must be eliminated or minimized by any technique is pinholes in the resist.

Although CaGe containing materials presently have the best temperature properties, the coercivity and defect density are often higher than Ga substituted material. These undesirable properties have been associated with a Ca-containing second phase. Be^{2+} ions are being evaluated as an alternative to Ca^{2+} for charge compensation. Initial films containing Be and Ge ions were in compression suggesting that insufficient Be had been incorporated. It seems expedient at this point to study the solubility of BeO in $PbO-B_2O_3$ flux before proceeding further.

Four types of multilayer structures were analyzed. The triple layer structures with a biasing or capping layer in between the bubble films seem to have the best properties. Several films with the biasing layer type structure have been grown and will be evaluated in the next period.

Yield is always an important consideration for a large capacity chip. An on-chip modification scheme is proposed with the hybrid chip organization. An electronic scheme is certainly not excluded but would not be suitable by itself for a large capacity chip. A modification yield of 1 is assumed in this analysis since the modification is made to only non-critical conductor paths on the redundant paths. Considering each chip to be composed of M subchips and each subchip of ℓ loops and each loop of g+r sections where r is the redundancy, to achieve a 90 percent loop yield within any subchip requires about a 20 percent loop redundancy or that there be 12 sections in each loop.

All the half disk retarding type switches required for decoding were found to work. The best one had a half period width conductor situated at the input half of the disk element. The minimum current was about 22mA and the phase margin was better than 180 degrees. Both one and two bit delay times were achieved.

FOREWORD

This is the third Interim Report on Contract F33615-76-C-1198 covering the period 4 May 1977 to 4 November 1977. The first interim report, AFAL-TR-77-17, covers the period 4 May 1976 to 4 November 1976 and the second interim report, AFAL-TR-77-198 covers the period 4 November 1976 to 4 May 1977. The research effort was performed in the Applied Magnetics and Solid State Materials Research Branches of the Physical Sciences Department. Dr. P. J. Besser is the Program Manager and Principal Investigator. Other major contributors to the program for this interval and their areas of effort are: Dr. D. M. Heinz, Materials Research, Dr. T. Kobayashi, Multilayer Structures, and Dr. T. T. Chen, High Capacity Device Development. Dr. L. R. Tocci contributed to the preparation of this report and will act as principal investigator for the remainder of the program.

LEVEL II

DDC

RECEIVED
NOV 2 1978
D

iii

TABLE OF CONTENTS

LIST OF ILLUSTRATIONS

SECTION I

INTRODUCTION

The objective of this basic research effort is to demonstrate the feasibility of a new technology for all solid state large data base memories for airborne/spaceborne applications. The program scope is limited to demonstrating the feasibility of the device functions and bit density capabilities required to meet the system goals.

It is the objective of this program to advance one technology into development. Based on an evaluation of the present and potential capabilities of candidate solid state technologies to meet the system goals, magnetic bubble domain technology has been selected as the one to be pursued on this program.

The proposed approach makes use of small bubble materials, multilayer, self-biased materials and devices, wafer level integration using hybrid chip designs and fineline lithographic techniques for device fabrication. The effort on small bubble materials research was devoted to: (1) extending the useful temperature range of the 2 μm and 1 μm bubble diameter materials which were developed in previous report interval, (2) investigating film growth on 76 mm dia substrates, and demonstrating the capabilities of the materials by device operation. With successful accomplishment of the above three tasks the small bubbles portion of the materials research effort has been concluded. Materials research has concentrated on the means for improving the performances of self-biased bubble films and on an alternate to CaGe substitution in bubble films. The status of this effort is reported in Section II.

Section III goes into a more detailed analysis of multilayer structures, specifically the properties and parameters which affect the static stability conditions. Four types of structures are considered.

In the continuation of high capacity chip development, two areas are presented in Section IV, chip yield considerations and M-1088 test chip evaluation. Concerning yield a more detailed analysis has been undertaken specifically for the case of the proposed hybrid type chip organization with on-chip (conductor) modification. The test chip characterization focusses on the passive replicator, the exchange and transfer switches and in more detail the retarding switch so important in the decoder network required in the hybrid chip organization.

SECTION II

MATERIALS RESEARCH

During the past half year, materials work has been concentrated on means for improving the performance of self-biased bubble films and on an alternative to CaGe substitution in bubble materials. A major limitation to the use of self-biased films in meeting a system goal of this program is operating over the -55 to +125°C temperature range because of the large temperature sensitivity of self-biased bubble domains. Two means for reducing this temperature sensitivity are being investigated: The first has to do with determining the influence of the material parameters of biasing layers on self-biased bubble properties and the second has to do with determining the influence of material parameters of in-plane capping layers on self-biased bubble properties. Another important area for improving the performance of self-biased films is in the isolation of device chip regions by mesa-etching for which a new resist is being evaluated. The final research area has to do with the use of Ge-substituted bubble compositions. When compared with Ga-substituted bubble formulations, CaGe-containing bubble films generally have higher coercivities and a tendency to have a larger number of defects. Since both of these effects are probably due to Ca-containing precipitates, an alternative to Ca in Ge-substituted compositions has been investigated.

2.1 INVESTIGATIONS ON PERFORMANCE IMPROVEMENT OF SELF-BIASED MATERIALS

The self-biased bubble film studies being carried out on this program are an extension of earlier work by Uchishiba, et al (Ref. 1, 2, 3). The self-biased structure consists of a saturated garnet layer (layer 1 in Figure 1) covered by a bubble garnet layer (layer 2 in Figure 1). If the anisotropy field of layer 1, $H_A(1)$, is larger than the saturation magnetization, $4\pi M_s$, of either layer, then once saturated, the biasing layer will remain saturated until a magnetic field greater than $H_A(1)$ is applied in the opposite direction. (The nucleation field is generally smaller than $H_A(1)$ at the edge of an as-grown wafer or of a sample mechanically cut from a wafer; however it can be made as large as $H_A(1)$ by use of a chemical etch to remove the edges.) A 180 deg domain wall separates layers 1 and 2. When the wall energy of layer 1, $\sigma_w(1)$, is greater than that of layer 2, $\sigma_w(2)$, the bubble capping wall is just inside layer 2. As

[1] H. Uchishiba, H. Tominaga, T. Namikata, and S. Sakai, "Internal Bias Effect of Double Layer Epitaxial Garnet Films" IEEE Trans. Magn. MAG-9, 381 (1973).

[2] H. Uchishiba, H. Tominaga, T. Obakata, and T. Manikata, "Growth and Properties of Stable Self Biasing Double Layer Epitaxial Garnet Films," IEEE Trans. Magn. MAG-10, 480 (1974).

[3] H. Uchishiba, H. Tominaga, and K. Asama, "Temperature Stable Self-Biasing Bubbles in Double Layer Films," IEEE Trans. Magn. MAG-11, 1079 (1975).
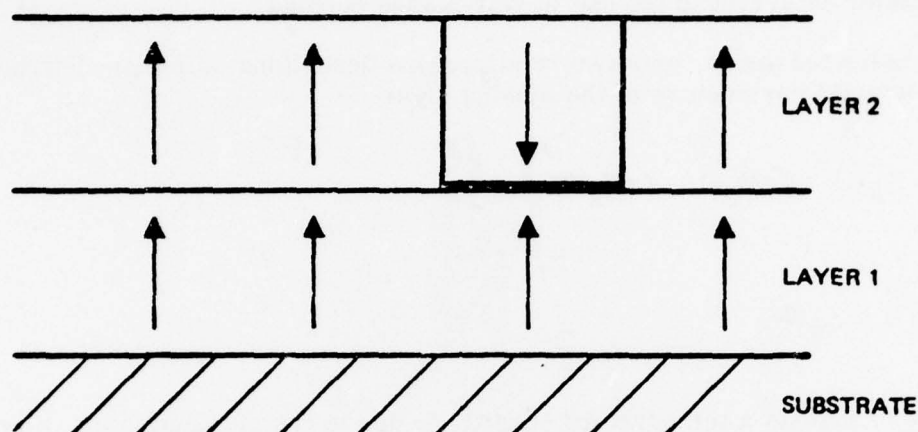
Figure 1. Double Layer Self-Biased Bubble Domain Structure

developed in the analysis of self-biased structures in an earlier Interim Report[4], associated with the formation of the bubble capping wall is an effective bias field, H_{eff}, which is given by

$$\frac{H_{eff}}{4\pi M_s} = \frac{\ell}{2h} \left(1 - \frac{1}{q}\right)^{1/2}$$

where ℓ is the characteristic length, h is the layer thickness and q is the quality factor. All of these material parameters refer to the bubble film, layer 2 in Figure 1. It was also shown in Ref. 4 that complete self-biasing of a bubble material with a q of 4 requires that (h/ℓ) of the bubble material lies in the range of 2.25 to 2.70.

In a self-biased structure, the temperature dependence of bubble diameter is strongly influenced by the presence of the biasing layer. The temperature coefficient

---

[4]P. J. Besser, T. T. Chen, D. M. Heinz, and T. Kobayashi, "High Density Magnetic Bubble Memory Techniques," Interim Report for 4 May 1976 to 4 November 1976, AFAL-TR-77-17, April 1977.

3

of bubble diameter, $d_T \equiv 1/d \; \partial d / \partial T$, and the temperature coefficient of characteristic length, $\ell_T \equiv 1/\ell \; \partial \ell / \partial T$, in an isolated bubble layer are related by $d_T = \ell_T$, but in a self-biased structure are related by $d_T = -A\ell_T$ where the coefficient, A, depends on the value of (h/ℓ) in layer 2. The magnitude of A has been found to vary between 2.7 and 12 (Ref. 3). This large temperature sensitivity of self-biased bubble diameter is a major deterrent to the use of self-biased bubbles.

As indicated above, only two relationships describing self-biased structures contain material parameters of the biasing layer:

$$H_A(1) > 4\pi M_s(1), \; 4\pi M_s(2)$$

and

$$\sigma_w(1) > \sigma_w(2),$$

and neither suggests a temperature sensitivity due to the biasing layer. However, earlier work at Rockwell International showed that the temperature behavior of self-biased bubbles is strongly influenced by properties of the biasing layer. One of the current studies is designed to provide greater insight into the influence of the biasing layer material parameters on self-biased bubble properties, in particular, the temperature sensitivity of bubble diameter.

A second study, also concerned with the temperature sensitivity of self-biased bubbles, involves triple layer films. In these structures, a third layer with in-plane magnetization (layer 3 in Figure 2) covers the saturated and bubble layers (layers 1 and 2 in Figure 2). Earlier investigations at Rockwell International on hard bubble suppression with in-plane magnetization layers on bubble films (Ref. 5 and subsequent studies) showed that ℓ_T was reduced to as little as 0.3 of its value for a bubble film alone. Preliminary work with triple layer self-biased films (as in Figure 2) have shown that an in-plane magnetization layer on a self-biased bubble film decreases d_T. The current study is therefore designed to provide insight into the influence of the material parameters of the in-plane magnetization layer on self-biased bubble properties.

The make-up of multilayer structures is conveniently described by a notation system which consists of a symbol for each layer arranged in the sequence that the films are deposited. The symbols are B for magnetic bubble layer, S for saturated magnetic layer (with magnetization perpendicular to the plane of the wafer) used in self-biasing and P for planar magnetic layer (with magnetization parallel to the plane of the wafer). Thus, the structure shown in Figure 1 is SB and the structure shown in Figure 2 is SBP.

[5] R. D. Henry, P. J. Besser, R. G. Warren and E. C. Whitcomb, "New Approaches to Hard Bubble Suppression," IEEE Trans. Magn. MAG-9, 514 (1973).
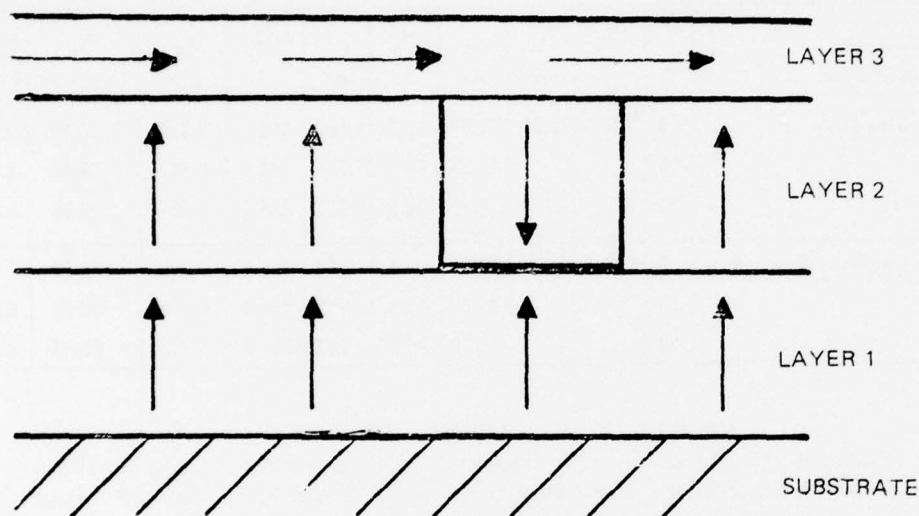
Figure 2. Triple Layer Self-Biased Bubble Domain Structure

2 1.1 Study of Biasing Layer Material Parameters

Since few material parameters of the biasing layer are treated explicitly by the present model for self-biased films, this study is directed toward determining their influence on self-biased bubble properties in order to improve temperature stability. For this investigation, a single bubble film composition and thickness was used on a series of biasing layer films having different values of thickness, saturation magnetization, uniaxial anisotropy, K_u, and Neel temperature, T_N, in order to isolate the effects of the biasing layer material parameters.

Biasing layer films with substantially different T_N values were produced using two melt formulations having the nominal compositions of $Er_{2.2}Eu_{0.8}Fe_{4.2}Ga_{0.8}O_{12}$ and $Er_{1.87}Eu_{0.47}Ca_{0.66}Fe_{4.34}Ge_{0.66}O_{12}$. Several growth rates were used to vary $4\pi M_s$ and K_u, and several film thicknesses were used. Following growth of these films. they were characterized at 0, 25 and 50°C. Typical values are presented in Table 1.

In preparing self-biased bubble films for evaluation with 16 µm period device patterns, it is necessary to choose the bubble film material parameters carefully. For a bubble material with a $4\pi M_s$ of ~200G, the biasing field margin is ~0.7($4\pi M_s$) = 14 0e. Since the permalloy device pattern provides a negative bias of about 10 0e, the self-biasing condition of a bubble should be 10/14 (=0.714) of the way between bubble domain collapse and bubble domain stripout. A plot of self-biasing conditions calculated with Thiele's force function was presented in a previous Interim Report

5

TABLE 1. TYPICAL PROPERTIES OF BIASING LAYER FILMS

Composition Film Number	t °C	T_N °C	h μm	W μm	H_0 Oe	ℓ μm	$4\pi M_s$ G	σ_w erg/cm³	K_u k erg/cm³	H_A k Oe	q
$Er_{2.2}Ev_{0.8}Fe_{4.2}Ga_{0.8}O_{12}$	0	182.3	1.91	29.85	10.2	1.692	215.2	0.624	86.14	10.06	48.6
	25			12.38	21.2	1.171	192.9	0.347	28.14	3.67	19.0
	50			8.89	30.8	0.975	205.2	0.327	26.79	3.28	16.0
$Er_{1.87}Ev_{0.47}Ca_{0.66}Fe_{4.34}Ge_{0.66}O_{12}$	0	219.7	1.97	43.82	8.5	1.957	250.4	0.976	175.10	17.57	70.2
	25			20.96	14.4	1.511	210.2	0.531	53.30	6.37	30.3
	50			12.70	22.5	1.203	203.4	0.396	30.73	3.80	18.7

(Ref 6). On this plot, 0.714 of the way between collapse and stripout on the q=5 line for a single-biased bubble film, the value of (d/h) is about 3.72 and the value of (ℓ/h) is about 0.381. The 16 μm period device pattern has a preferred d of about 3.70 μm so that the required h = 1.00 μm and ℓ = 0.381 μm.

All single layer bubble films must meet close tolerances on stripwidth, w, and collapse field, H_{col}, for use in devices. Film growth procedures have been worked out to produce large numbers of bubble films with near-identical w and H_{col} properties. For self-biased structures, h and ℓ must meet close tolerances. Since h is determined by the growth period and the growth rate, control of the growth rate becomes more critical for self-biased bubble films.

In preparing this series of self-biased films we have found that the continuous loss of PbO from the melt is a controlling factor in meeting h and ℓ requirements. Loss of PbO increases the growth rate which results in (a) the deposition of thicker films during the same growth period, and (b) the incorporation of less Ga, causing $4\pi M_s$ to increase. These changes affect ℓ and other parameters as well.

The nominal composition of the bubble film used in these studies is $Y_{2.6}Sm_{0.4}Fe_{3.8}Ga_{1.2}O_{12}$. The procedure that was developed for growing the bubble layers for this group of self-biased films consisted of the following: First, the melt was adjusted so that a test film grown on a GGG substrate had desirable bubble properties such as those presented in Table 2. Then bubble films were grown in rapid sequence on from two to four wafers for the self-biasing study. Finally, a second test film was grown on GGG. The value of ℓ and the other properties of the bubble films were assumed to lie between those of the two test films.

[6] P. J. Besser, T. T. Chen, D. M. Heinz and T. Kobayashi, "High Density Magnetic Bubble Memory Techniques," Interim Report for November 4, 1976 to May 4, 1977, AFAL-TR-77-198, October 1977.

TABLE 2. TYPICAL PROPERTIES OF A BUBBLE GARNET FILM

Composition Film Number	t °C	T_N °C	h μm	W μm	H_0 Oe	ℓ μm	$4\pi M_s$ G	σ_w erg/cm²	K_u erg/cm³	H_A kOe	q
$Y_{2.6}Sm_{0.4}Fe_{3.8}Ga_{1.2}O_{12}$	0	128.5	1.049	4.30	34.9	0.495	207.2	0.169	8.98	1.09	5.26
	25			3.84	36.9	0.459	197.7	0.143	7.24	0.92	4.65
8-7-79/U	50			3.20	38.8	0.403	176.8	0.100	4.24	0.60	3.41

At the end of each day, PbO was added to make up for its loss during the past 24 hr. At the start of the next work day, a test film was grown on GGG. If the properties were satisfactory, additional bubble films were grown for self-biased structures. If the properties were not satisfactory, growth conditions were altered until a test film with the desired properties was produced. Then additional self-biased films were grown.

The thickness of each film in the self-biased structure was determined using the standard infrared interferometric technique (assuming that the index of refraction of each magnetic garnet layer is 2.10 in the wavelength region used). The thickness of the biasing layer was measured after it was grown. Then the thickness of the double layer was measured, and the thickness of the bubble film was obtained by taking the difference. This bubble film thickness and the characteristic length of test films grown during the same film growth sequence constitute the bubble film characterization.

A group of nine 38-mm diameter SB wafers were prepared for this study. Before the effects of varying the material parameters of the S layers can be evaluated, the wafers must be mesa-etched to isolate these layers from domain-nucleation defects. A decision on the etching resist technique to be employed is awaiting the completion of experiments with a new resist described in para 2.1.3.

2.1.2 Study of In-plane Magnetization Layer Material Parameters

In the self-biased structure, bubbles are more temperature sensitive than they are in single layer films of the same composition. Earlier work at Rockwell International showed that the addition of an in-plane magnetization layer over a bubble film reduced the temperature sensitivity of those bubbles. Thus we are investigating the SBP structure shown in Figure 2 to determine the effect of an in-plane magnetization layer on the temperature dependence of self-biased bubbles. For this study, a standard biasing layer and bubble layer were used with a series of in-plane magnetization layer films having different values of thickness, saturation magnetization, Neel temperature and film-substrate lattice parameter mismatch, in order to isolate the effects of these material parameters.

Garnet is a cubic material so that an in-plane magnetic moment is not the result of crystalline anisotropy. Instead, an in-plane magnetic moment is induced in an epitaxial garnet film by the inverse magnetostriction effect. The lattice parameter mismatch, Δa, between film lattice parameter a_f, and the substrate

lattice parameter, a_s, is defined by $\Delta a = a_s - a_f$. When $a_f > a_s$, the film is constrained by the massive substrate to match a_s, placing the layer in a state of lateral compression. (Individual films in a multilayer structure are in compressive or tensile stress depending on their respective a_f values.) The stress, σ, induced by the lattice parameter mismatch is given by

$$\sigma = \frac{Y}{1-\mu} \left(\frac{\Delta a}{a_f} \right)$$

where Y is Young's modulus, and μ is the Poisson ratio of the film. For a garnet with a negative magnetostriction constant, λ_{111}, compressive stress induces planar magnetic anisotropy, K_u^S, given by

$$K_u^S = -\frac{3}{2} \sigma \lambda_{111}.$$

Thus, the amount of in-plane anisotropy in an epitaxial garnet film on a GGG substrate is determined by a_f and λ_{111}, both of which are composition-dependent.

At Rockwell International, films of $(YGd)_3Fe_5O_{12}$ with $a_f > a_s$ have been used as in-plane magnetization layers in the past (Ref. 5). However, the Gd makes the properties of the garnet film quite temperature sensitive, which might obscure the influence of the in-plane magnetization layer on self-biased bubbles. Since Gd was used to increase a_f sufficiently to place the film in compression, another large ion may serve this purpose equally well and we have used La instead of Gd in films for this investigation.

The biasing layer for this study was $2\,\mu m$-thick $Er_{2.2}Eu_{0.8}Fe_{4.2}Ga_{0.8}O_{12}$ and the bubble layer for this study was $1\,\mu m$-thick $Y_{2.6}Sm_{0.4}Fe_{3.8}Ga_{1.2}O_{12}$. Film growth procedures similar to those used for preparing the SB films were used. The first in-plane magnetization layer had a nominal composition of $Y_{2.92}La_{0.08}Fe_5O_{12}$. Growth conditions were selected to grow films of this material in compression with a Δa of $-0.0023A$ and a group SB of wafers were coated with different thicknesses of this composition. The melt was then modified by additions to produce films having a nominal composition of $Y_{2.90}La_{0.10}Fe_{4.4}Ga_{0.6}O_{12}$. Growth conditions were selected to grow films of this material in compression with a Δa of -0.0040Å and a group of SB wafers were coated with different thicknesses of this composition. Two additional growth conditions will be selected to provide different amounts of compressive stress on additional samples.

We were able to alter the amount of stress between film and substrate by altering growth conditions. The large La ion increases the film lattice parameter while the small Ga ion decreases the film lattice parameter. Also, the distribution coefficients go in opposite senses with changing growth rate: The La in the film increases with growth rate and the Ga in the film decreases with growth rate. This method for changing stress also changes the magnetization of the film due to the varying Ga content; however, we expect to be able to separate the parameters influencing the bubble properties.

A group of eight 38-mm diameter SBP wafers are being prepared for this study. As with the SB wafers, before the effects of the P layers can be evaluated,

8

the wafers must be mesa-etched to isolate the biasing layers from domain-nucleating defects. Evaluation will progress when experiments with the new resist for etching have been completed.

2.1.3 Study on Resists for Mesa Etching

In self-biased bubble structures, it is necessary to isolate the biasing film from edge defects in order to achieve a saturated (single domain) state (Ref. 2). For use in device studies, the etching process involves definition of a resist pattern and chemical etching of the garnet. During our earlier study of etching self-biased films into mesas using sputtered SiO_2 as the resist to hot H_3PO_4 (Ref. 6), we encountered small domain-pinning defects which appeared to be due to pits in the bubble layer. These pits were attributed to pinholes in the mask pattern and/or the SiO_2 resist. To overcome either source of pinholes, the resist deposition and masking processes were repeated with the expectation that any pinhole in one step would be terminated at the second step. As a result of these procedures, the number of defects was decreased (Ref. 6) but the increased processing steps are cumbersome and time consuming.

A recent paper described the use of an organosilicon solution to form a resist for garnet etching (Ref. 7). Organosilicon solutions are marketed for diffusion-doping of semiconductors and are applied by spinning-on and baking at $900^\circ C$. Two preliminary experiments were carried out on garnet wafers which were coated with organosilicon and baked. The first garnet wafer was etched for five minutes in hot H_3PO_4 and pitting was only observed near the wafer edge. (The normal mesa-etching period is 15 seconds in hot H_3PO_4.) The second garnet wafer had the baked organosilicon photolithographically patterned into die-sized areas and it was etched for three minutes in hot H_3PO_4. Again pitting was observed chiefly near the wafer edge; however, a few additional pits were found. The ability of this readily-applied resist to withstand extended periods in hot H_3PO_4 makes it an attractive alternative to sputtered SiO_2.

A final evaluation experiment is underway in which a wafer which has been coated, photolithographically patterned, and etched, is having device circuits processed on the mesas. Should this processing procedure prove to be satisfactory, the SB and SBP wafers will be processed using this new resist.

2.2 INVESTIGATION ON ALTERNATIVES TO CaGe SUBSTITUTION IN BUBBLE MATERIALS

In bubble garnet compositions, the magnetic moment is adjusted to produce the desired bubble diameter by substitution of nonmagnetic ions for Fe^{3+} ions. To minimize the amount of substitution and thereby keep T_N as high as possible, the non-magnetic ion should substitute solely for Fe on tetrahedral (d) sites in the garnet crystal lattice. Ga-substituted bubble compositions with about one Ga per garnet formula unit have about 90 percent of the Ga on d sites and the remaining 10 percent on octahedral (a) sites (Ref. 8). This a site substitution counteracts part of the d site

[7] M. Nemiroff and H. Yue, "La:YIG Disks on GGG Substrates for Microwave Applications," IEEE Trans. Magn. MAG-13, 1238 (1977).

[8] S. Geller, "Crystal Chemistry of the Garnets," Z. Krist. 125, 1 (1967).

substitution, as well as lowering T_N. Ge-substituted LPE bubble compositions have about 98 percent of the Ge on $\underline{d}$ sites and about 2 percent on $\underline{a}$ sites (Ref. 9), so that Ge is more efficient than Ga in lowering $4\pi M_S$. Since the Ge^{4+} ions substitute for Fe^{3+} ions, an equal number of divalent ions must substitute for other trivalent ions to realize charge neutrality. Ca^{2+} is normally used to charge compensate Ge^{4+} in bubble garnet compositions, where Ca^{2+} replaces Y^{3+} or a rare earth ion on a dodecahedral ($\underline{c}$) site. Currently, the best bubble materials for use at elevated temperatures are CaGe-substituted.

Unfortunately, the coercivity and defect density in CaGe-substituted compositions are often higher than in Ga-substituted compositions. These undesirable properties of Ca-containing garnets have been associated with the presence of a Ca-containing second phase in bubble films (Ref. 10). A survey of other divalent ions which might be used to charge compensate Ge^{4+} fall into three categories:

1) Ions that occupy $\underline{c}$ sites (and probably have more limited solubility in garnets than Ca^{2+}): Sr^{2+}, Ba^{2+}, Pb^{2+}, Cd^{2+} and Hg^{2+},

2) Ions that occupy $\underline{a}$ sites (Ref. 8) (which is undesirable): Mn^{2+}, Fe^{2+}, Co^{2+}, Zn^{2+}, Ca^{2+}, Mg^{2+} and Ni^{2+}, and

3) Ions that probably occupy $\underline{d}$ sites: Be^{2+}.

Thus, in attempting to alleviate the coercivity and defect density problems (and possibly to improve other bubble properties as well), on this program Be^{2+} is being evaluated as an alternate ion to Ca^{2+} for charge-compensating Ge^{4+}.

Perhaps due to its small ionic size or to its reputation as a toxic agent, Be has not been reported as a constituent of garnets heretofore. In tetrahedral coordination, the effective ionic radius of Be^{2+} is 0.27Å which is quite small compared with the radius of Fe^{3+}, 0.49A (Ref. 11). However, the radii for Si^{4+} and B^{3+} (from the flux) are 0.26 and 0.11A (Ref. 11) and Si^{4+} has been reported in a number of garnet compositions (Ref. 8), while B^{3+} has been shown to have been incorporated in garnet films (Ref. 12). There is thus reasonable certainty that Be^{2+} should enter the garnet lattice and reside exclusively on $\underline{d}$ sites, like Si (Ref. 8).

The presence of equal numbers of Be and Ge ions on $\underline{d}$ sites means that only half the amount of Ge used in CaGe substitution need be present in BeGe substitution

[9] S. L. Blank, J. W. Nielsen and W. A. Biolsi, "Preparation and Properties of Magnetic Garnet Films Containing Divalent and Tetravalent Ions," J. Electrochem. Soc. 123, 856 (1976).

[10] M. Kestigian, A. B. Smith, and W. R. Bekebrede, "Magnetic Inhomogeneities in $(YSmCa)_3(FeGe)_5O_{12}$ and Their Elimination by Improved Growth Procedures," Mat. Res. Bull. 11, 773 (1976).

[11] R. D. Shannon, "Revised Effective Ionic Radii and Systematic Studies of Interatomic Distances in Halides and Chalcogenides," Acta Cryst. A32, 751, (1976).

[12] S. L. Blank, W. A. Biolsi and J. W. Nielsen, "The Effect of Melt Composition on the Curie Temperature and Flux Spin-Off from Lutetium Containing LPE Garnet Films," IEEE Trans. Magn. MAG-13, 1095 (1977).

to attain the same magnetic moment. Since 2 percent of the Ge is on $\underline{a}$ sites while all of the Be is on $\underline{d}$ sites, there would be less $\underline{a}$ site substitution in BeGe compositions than in CaGe compositions. The difference in $\underline{d}$ site substitution between Ge and Ga is (98-90=) 8 percent, which for materials with $4\pi M_S$ values of 400 to 500 G results in T_N differences of about $50^O C$. The difference in $\underline{d}$ site substitution between BeGe and CaGe is (99-98=) one percent, which should result in a T_N difference of ($50^O C/8$ percent =) $6^O C$. Thus, BeGe compositions should have T_N temperatures several degrees higher than CaGe compositions.

A consequence of the absence of Ca from BeGe compositions is that the $\underline{c}$ sites are completely available for rare earth ion occupancy. This may become important in obtaining higher growth-induced anisotropies for smaller bubbles by the use of greater concentrations of rare earth ions. Also, since charge compensation should take place locally, there is a high probability that Be^{2+} and Ge^{4+} ions occupy nearest neighbor $\underline{d}$ sites. This would undoubtedly cause large local variations in the crystalline field which might also contribute to the growth-induced anisotropy.

Substitution of a small ion for Fe causes a contraction of the lattice parameter. An analysis of the lattice parameters for CaSi compositions (Ref. 13) shows that the substitution of one Si for one Fe per garnet formula unit causes a lattice parameter change of $-0.16Å$. Due to the slightly larger size of Be, substitution of one Be for one Fe per garnet formula unit would cause a lattice parameter change of about $-0.155Å$. A similar analysis of the lattice parameters for CaGe compositions (Ref. 13) shows that the substitution of one Ge for one Fe per garnet formula unit causes a lattice parameter change of $-0.08Å$. Thus, the equivalent substitution for one Fe of 0.5 Be +0.5 Ge per garnet formula unit would cause a lattice parameter change of $(-0.155Å-0.08Å)/2 = -0.12Å$. For epitaxial growth of bubble films on GGG substrates, a desirable lattice parameter mismatch is $0.003Å$ so that it is necessary to have compensating large ions on $\underline{c}$ sites to expand the lattice and compensate for BeGe substitution.

Last year an experiment was carried out at Rockwell International to determine the influence of a small amount of BeO in a bubble garnet melt. The addition of 0.68 mole percent of BeO to the solute of a $(YSmCa)_3 (FeGaGe)_5 O_{12}$ melt caused the following changes in film properties: a decrease of a_f of $0.0012Å$, a decrease in $4\pi M_S$ of 21G, and a decrease in T_N of $3.8^O C$. The lattice parameter change and the $4\pi M_S$ change suggest that there is about 0.01 Be per garnet formula unit, while the T_N change suggests that there is about 0.3 Be per garnet formula unit. Wet chemical analysis revealed about 0.002 Be per garnet formula unit. (The discrepancies are difficult to interpret because of experimental uncertainties.)

Distribution coefficients for Be (α_{Be}) were estimated from these film concentrations. Based on chemical analysis, $\alpha_{Be} \simeq 0.042$; based on changes in a_f and $4\pi M_S$, $\alpha_{Be} \simeq 0.28$; and based on change in T_N, $\alpha_{Be} \simeq 8.4$. This spread in α_{Be} values makes them too uncertain to be of use in formulating a melt. However, the

---

[13] S. Geller, H. J. Williams, G. P Espinosa and R. C. Sherwood. "Importance of Intrasublattice Magnetic Interactions and of Substitutional Ion Type in the Behavior of Substituted Yttrium Iron Garnets." Bell System Tech. J. 43, 565 (1964).

experiment established the fact that the small Be^{2+} ion entered the garnet lattice as anticipated.

Nothing was available from the literature on the solubility of BeO in the $PbO-B_2O_3$ flux system normally used for liquid phase epitaxy (LPE) of garnet films. The only relevant data was that BeO single crystals had been grown from a PbO melt (Ref. 14), implying that there is sufficient solubility at an elevated temperature to permit crystal growth on cooling.

The garnet composition $Eu_2YFe_{4.34}Be_{0.33}Ge_{0.33}O_{12}$ was selected for evaluating BeGe substitution. This composition should be in slight tension on GGG ($\Delta a \simeq 0.001\text{Å}$), have a $4\pi M_S$ of 240G for 4 μm bubbles, and have a T_N of 200°C. Since neither the distribution coefficient nor the solubility of Be was known, a melt was formulated with a small amount of BeO with the intent of adding BeO as needed. (The toxicity of BeO precludes its handling as a powder so that it was necessary to add pieces of crystallized BeO to the melt.) The initial melt had a solute molar concentration (R_4) of 11.4 percent with an estimated garnet saturation temperature of about 945°C.

The initial garnet films were in compression, implying that an insufficient amount of Be and Ge ions had been incorporated into the film. Several BeO additions were made but the entire sequence of films grown in this study were in extreme compression (indicated by faceted growth). This may be attributed to too much of the large Eu ions and not enough of the small ions in the films.

Following initial melt formulation and each BeO addition, the melt temperature was raised to 1200°C for a sufficient time to bring all floating solids into solution. Then the temperature was lowered for film growth. After several BeO additions, it was found that microscopic hexagonal BeO platelets nucleated and grew on the surface of the melt at about 1050°C, showing a limited solubility for BeO in the $PbO-B_2O_3$ flux. At this temperature, the melt was not saturated with respect to the garnet phase so that a film did not grow on GGG at this temperature. Thus the melt behaved more like a pseudo-ternary system (composed of flux, garnet and BeO) rather than a pseudo-binary system (composed of flux and garnet) of a typical LPE melt. In formulating the melt, it had been assumed that the solubility of BeO was sufficient to provide the necessary Be concentration for film growth of the desired composition in the presence of the concentrations of the other ions, but this assumption was in error. The solubility of BeO was somewhat lower than that of the other oxides normally used in LPE garnet growth.

In endeavoring to gain results rapidly, we attempted to grow a bubble composition with insufficient solubility information. The next portion of this study will determine the solubility limits of BeO in $PbO-B_2O_3$ flux. This will permit a melt to be formulated with a lower solute concentration which should yield the desired film composition.

---

[14] R. C. Linares, "Growth of Refractory Oxide Single Crystals," J. Appl. Phys. **33**, 1747 (1962).

SECTION III

MULTILAYER STRUCTURES

The analysis of multilayer structures was expanded to include four types of structures. These included one type which has purely magnetostatic coupling between the two layers, two which are principally magnetostatic, and one which is directly exchange coupled. For double bubble encoding these structures must satisfy several requirements. For stable "1" and "0" states the double and single bubbles must coexist stably over a reasonable range of external bias field. Also the double and single bubbles must have practically the same diameter when a mixture of them forms a hexagonal lattice. Lastly, the domain must be able to propagated by suitable means and the above characteristics must be the same under dynamic conditions.

The stability characteristics are discussed for each type of structure and then the analysis is carried through mathematically. The type 2 structure is taken as an example and the calculations are carried through to show how the proper characteristics can be obtained.

A number of type 2 films (double bubble self-biased) have been grown. Before this growth, individual films for each layer were grown and characterized to establish the proper parameters. The double bubble films are presently being evaluated.

3.1 CLASSIFICATION OF MULTILAYER STRUCTURES

The basic configuration of the multilayer structures under consideration is illustrated by the solid lines in Figure 3. It consists of two epitaxial ferrimagnetic garnet films (layers 1 and 2) separated by a magnetic or nonmagnetic intermediate layer. Layers 1 and 2 are predominantly uniaxial with their easy axes perpendicular to the film plane. One layer, which can be considered as a carrier layer, supports a hexagonal close packed array of bubble domains (bubble lattice). The second layer, which can be considered as a data layer, supports bubble domains ("1" states) and vacancies ("0" states) to represent binary information. Depending on the properties of the intermediate layer, multilayer structures can be classified into four types as shown in Table 3.

Type 1 has a nonmagnetic intermediate layer. Thus the coupling between layers 1 and 2 is purely magnetostatic.

Type 2 has a magnetic intermediate layer which is "permanently" magnetized antiparallel to the magnetization of the carrier and data domains. It is exchange-coupled to layers 1 and 2. Consequently a 180 deg domain wall (called a "capping wall") is formed at the interface of the intermediate layer and a carrier or data domain. However, the coupling between layers 1 and 2 is essentially magnetostatic since the intermediate layer is saturated in one direction and its permeability is nearly equal to that of vacuum.
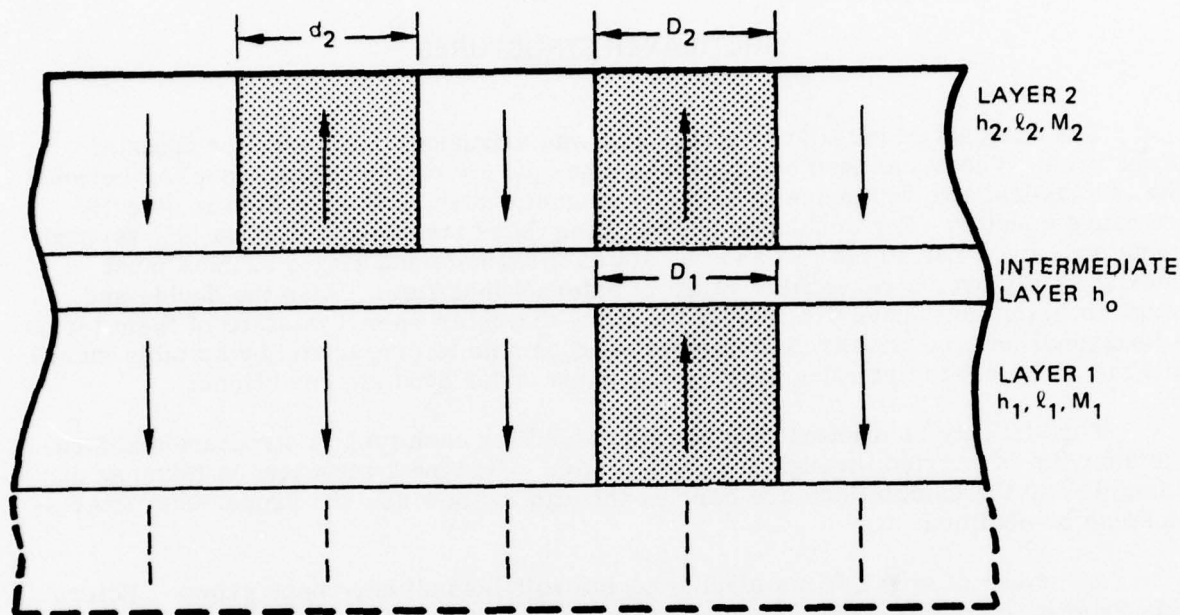
13

Figure 3. Multilayer Structure of
Coupled Magnetic Domains

The intermediate layer of Type 3 is also magnetic but its magnetization lies in the plane of the layer (Ref. 15). Therefore, a 90 deg domain wall is formed at the interfaces with layers 1 and 2. The coupling between layers 1 and 2 is also magneto-static but the in-plane permeability of the intermediate layer is rather high since it is not saturated.
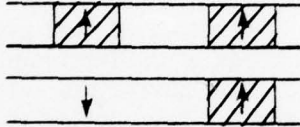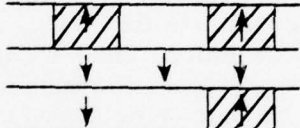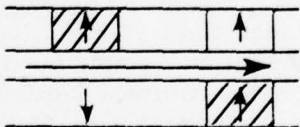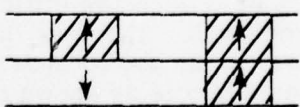
Type 4 has no intermediate layer. Layers 1 and 2 are directly exchange-coupled.

3.2 PROPERTIES OF MULTILAYER STRUCTURES

In order that a multilayer structure be used for our lattice file medium, it must satisfy a number of requirements other than those imposed on conventional bubble materials. One such requirement is the static stability of the "1" and "0" states. For the bubble lattice this means that double and single bubbles must coexist stably over a reasonable range of an external bias field. Another such requirement is the uniformity of a bubble lattice under random distributions of data bubbles. This implies that double and single bubbles must have practically the same diameter when a mixture of them forms a hexagonal lattice.

---

[15]R. D. Henry, P. J. Besser, R. G. Warren, and E. C. Whitcomb, "New Approaches to Hard Bubble Suppression," IEEE Trans. Magn. MAG-9, 514 (1973).

TABLE 3. CLASSIFICATION OF MULTILAYER STRUCTURES

	Properties of Intermediate Layer	Types of Coupling Between Layers 1 and 2	Schematic
1	Nonmagnetic	Magnetostatic	
2	Magnetic with the magnetization antiparallel to that of carrier and data domains	Magnetostatic-Exchange	
3	Magnetic with the magnetization in the plane of the film	Magnetostatic-Exchange	
4	Zero thickness	Exchange	

Additionally, the domain structures must be able to be propagated with appropriate driving means. And of course, these domain structures must meet the above-mentioned requirements under dynamic conditions as well. Mainly with the basic static requirements in mind, let us briefly examine each structure. For simplicity, it is assumed in the following that layers 1 and 2 correspond to the data and carrier layers, respectively, unless otherwise noted.

For the purposes of illustration let us consider the Type 1 structure and examine how the magnetostatic interaction affects the stability of the domains in each layer.

15

First, let us look at the bubble/bubble coupling. Unless the magnetizations (M_1, M_2) and the characteristic lengths (ℓ_1, ℓ_2) of the two layers are considerably different from each other, the qualitative behavior of coupled bubbles does not change appreciably from that of the case when they are identical with each other $(M_1 = M_2$ and $\ell_1 = \ell_2)$. Thus for simplicity let us assume that layers 1 and 2 are identical except for the thicknesses (h_1, h_2) and that $h_1 < h_2$.

First of all, the properties of a single bubble in layer 2 are independent of the thickness of the intermediate layer, h_o, and identical with that of a bubble in a single layer film having the same material parameters. Also, if h_o is large compared to h_1 and h_2, the bubbles in layers 1 and 2 behave independent of each other according to the stability conditions determined by their respective thicknesses. On the other hand, if $h_o = 0$, a double bubble behaves like a single bubble with the effective thickness, h^*, equal to $h_1 + h_2$, and the diameters, D_1 and D_2 of the bubbles in layers 1 and 2 are identical. For an intermediate value of h_o, a double bubble can exhibit a mixed behavior of a single bubble and two separate bubbles. In other words, as the external bias field, H_B, is increased, a double bubble first behaves like a single bubble with $h^* < h_1 + h_2$ and $D_1 \approx D_2$ but as H_B is further increased and reaches a critical value, the bubble in the thinner layer (layer 1) collapses and the bubble in the thicker layer (layer 2) abruptly shrinks its diameter. The rest of the behavior of the still existing bubble in the thicker layer is of course, that of a separate bubble. In short, the effective thickness of a double bubble, h^*, increases from h_1 to $h_1 + h_2$ as h_o decreases from infinity to zero. Thus, in this case the effective thickness increase is a good measure of the magnetostatic coupling strength. The effect of the layer 1 bubble on the layer 2 bubble (or vice versa) is to supply a field antiparallel to the bias field. Thus, in general, the diameter of a double bubble, D_2 is greater than that of a single bubble, d_2, for a given bias field. In order that $D_2 \approx d_2$ under the same external field, therefore, the effect of the layer 1 bubble must be small. This implies that h_1 must be small compared to h_2. If this is not the case, then h_o cannot be small compared to h_1.

The above requirement is not in our favor, since it becomes difficult to distinguish between the single and double bubbles (for detection) if h_1 is small compared to h_2 or it becomes difficult to manipulate the double bubble if the intermediate layer is too thick. There is, however, a way to ease this requirement. That is, a bias layer can be placed under layer 1 to "selectively" supply an effective bias field to the layer 1 bubble as shown by the dotted line in Figure 3. As will be shown in the following section, this self-bias field to the layer 1 bubble is equivalent to an external field of magnitude $\sigma_{1b}/2h_1 M_1$ where σ_{1b} is the energy of the "capping wall" described in the previous section (Ref. 16). The net effect of this self-bias field on the double bubble can be considered as an effective field, H_{eff}, of magnitude $\sigma_{1b}/2h^* M_s$ where h^* is the effective thickness of the double bubble and $M_s = M_1 = M_2$ in our example. This effective field of course makes the double bubble smaller. Thus, a proper choice of h_o, h_1, and h_2 can make the single and the double bubbles equal in diameter under the same external field (which may include neighboring bubble fields when closely packed) even when h_o is small and h_1 and h_2 are comparable.

---

[16]T. W. Liu, A. H. Bobeck, E. A. Nesbitt, R. C. Sherwood, and D. D. Bacon, "Thin-Film Surface Bias on Magnetic Bubble Materials," J. Appl. Phys. 42, 1360 (1971).

The effective field can as well eliminate the external bias field altogether to make the double bubble lattice completely self-biased. This can be done because the layer 2 bubbles (carrier bubbles) are stabilized by their mutual interactions whereas the layer 1 bubbles (data bubbles) can be stabilized by the self-bias layer.

An additional advantage of placing a bias layer at the bottom of layer 1 is that it suppresses hard bubbles in layer 1. Unlike layer 2, which can be ion-implanted, layer 1, once grown, cannot be accessed for hard bubble suppression by ion implantation. Some other methods such as annealing (Ref. 17) may have to be used for hard bubble suppression. There is also a possibility that successive growth of the intermediate layer and layer 2 might serve effectively as annealing.

The type 2 structure has a "built-in" bias layer. Since the coupling between the layer 1 and layer 2 domains is essentially magnetostatic, the domain behavior is quite similar to that of the type 1 structure except that the layer 1 and layer 2 domains are biased by the amount $\sigma_{10}/2h_1 M_1$ and $\sigma_{20}/2h_2 M_2$, respectively, where σ_{10} and σ_{20} are their respective interface capping wall energies.

Thus structure has several advantages over the type 1. First of all, complete self-biasing of the lattice can be achieved without an additional bias layer. More-over, the input/output (I/O) region can be made self-biased also and compatible with conventional I/O techniques. Another advantage is that the intermediate layer can suppress hard bubbles in both layers.

The intermediate layer of the type 3 structure can also suppress hard bubbles in both layers 1 and 2. Since this layer has a high permeability parallel to the film plane and a low permeability perpendicular to it, it produces complicated magnetostatic interactions between the layer 1 and layer 2 domains. For example, consider a single bubble in layer 2. For $h_0 = 0$, it is a single bubble with $h^* = h_2$. As h_0 increases, however, a considerable amount of the stray field of the bubble is absorbed by the intermediate layer and its collapse field increases, corresponding to $h^* > h_2$. As $h_0 \rightarrow \infty$, all the magnetic poles at the bottom surface of the bubble are absorbed. The situation approximately corresponds to the case in which a mirror image of the bubble is created at the bottom of the bubble. Thus the bubble behaves as though its thickness were doubled, i.e., $h^* \approx 2h_2$.

A similar argument can be applied to a double bubble. For $h_0 = 0$, it behaves like a single bubble with $h^* = h_1 + h_2$. As $h_0 \rightarrow \infty$ the double bubble breaks up into two uncoupled single bubbles having $h^* = 2h_1$ and $h^* = 2h_2$, respectively. An interesting situation arises when $h_1 = h_2$. In this case, this simple argument predicts that the collapse field of the double bubble or equivalently the effective thickness is independent of h_0 with $h^* = 2h_1 = 2h_2$. It should be noted, however, that the actual magnetostatic coupling weakens rapidly with increasing h_0. Thus, the effective thickness increase is not a good measure of coupling strength for the type 3 structure.

---

[17] R. C. LeCraw, E. M. Gyorgy, and R. Wolfe; "Suppression of Hard Bubbles in LPE Garnet Films by Inert Atmosphere Annealing," Appl. Phys. Lett. 24, 533 (1974).

Despite the complicated magnetostatic interactions the type 3 structure can provide a structure adequate for the double-bubble or stripe-bubble lattice. Again, it may be preferred to place a bias layer at the bottom.

The type 4 structure has only two layers but this advantage seems to be more than offset by other disadvantages. It should first be noted that a single bubble in layer 2 has a capping wall at the bottom. In order for this bubble to be stable against "run-through" (i. e., spontaneous extension of the domain in layer 2 through layer 1 to the substrate) the wall energy of layer 1 (σ_{w1}) must be greater than that of layer 2 (σ_{w2}). This requirement completely eliminates the possibility of using the same material for both layers. It should also be noted that the single bubble is biased by the capping wall whereas the double bubble is not. Thus, it seems very difficult, if not impossible, to make both single and double bubbles equal in size under a common bias field. The reason is that the single bubble has a lower collapse field even without the bias effect from the capping wall. Therefore, placing a bias layer at the bottom of layer 1 is a necessity. Nevertheless, the lattice uniformity requirement seems to be more difficult to meet in the structure than in the others.

3.3 ANALYSIS OF THE MULTILAYER STRUCTURES

Analyses of the stability of isolated single and double bubbles provide a basis for the stability and uniformity of the single/double-bubble lattice. In fact, it can be shown that if isolated single and double bubbles exhibit the same diameters under a common external bias field, they do form a uniform lattice in the close packed configuration. Accordingly, we will discuss here the stability of isolated single and double bubbles.

The coupling between layers 1 and 2 is essentially magnetostatic for the type 1 and type 2 structures and the equilibrium conditions can be treated together. The force equations similar to that of Thiele (Ref. 18) can then be written as

$$\text{Single:} \quad \frac{\ell_2}{h_2} + \frac{d_2}{h_2}\left(\overline{H}_{B2} + \overline{H}_{20}\right) - F\left(\frac{d_2}{h_2}\right) = 0 \tag{1}$$

$$\text{Double:} \quad \frac{\ell_2}{h_2} + \frac{D_2}{h_2}\left(\overline{H}_{B2} + \overline{H}_{21} + \overline{H}_{20}\right) - F\left(\frac{D_2}{h_2}\right) = 0 \tag{2}$$

$$\frac{\ell_1}{h_1} + \frac{D_1}{h_1}\left(\overline{H}_{B1} + \overline{H}_{12} + \overline{H}_{10} + \overline{H}_{1b}\right) - F\left(\frac{D_2}{h_2}\right) = 0 \tag{3}$$

---

[18] A. A. Thiele, "Theory of Cylindrical Magnetic Domains," Bell Syst. Tech. J. 48, 3287 (1969).

where, with i, j = 1 or 2,

$$\overline{H}_{Bi} = \frac{H_B}{4\pi M_i} \; ; \; \overline{H}_{io} = \frac{\ell_i}{2h_i}\left(1 - \frac{1}{q_i}\right)^{1/2} \; ; \; \overline{H}_{1b} = \frac{\ell_1}{2h_1}\left(1 - \frac{1}{q_1}\right)^{1/2}$$

$$\overline{H}_{ij} = -\frac{M_j}{M_i}\frac{D_j}{2h_i}\int_0^\infty J_0\left(\frac{kD_i}{2}\right)J_1\left(\frac{kD_j}{2}\right)\left(1 - e^{-kh_i}\right)$$

$$x\left(1 - e^{-kh_j}\right)e^{-kh_o}\frac{dk}{k}$$

In the above, $4\pi M_i H_{ij}$ is the z component of the stray field of the layer j bubble averaged over the wall of the layer i bubble (Ref. 19). $\overline{H}_{io}$ is the normalized effective bias field supplied to the layer i bubble from the intermediate layer (Ref. 20). $\overline{H}_{io}$ must be dropped for the Type 1 structure. $\overline{H}_{1b}$ is the normalized effective bias field supplied to the layer 1 bubble from the bias layer thereunder and must be dropped if the bias layer is absent.

The stability of the single bubble can be obtained by solving Eq (1) for d_2 as a function of H_B. The stability of the double bubble can be obtained by simultaneously solving Eqs. (2) and (3) for D_1 and D_2 as a function of H_B.

As discussed in the previous section, the magnetostatic interactions in the Type 3 structure are complicated. The effect of the planar magnetic layer on the single bubble is to increase its collapse field. A rigorous approach to analyzing this effect is extremely difficult. Fortunately, however, this effect can be approximately represented by an effective field that has a simple analytical form (Ref. 21). If

[19] W. F. Druyvesteyn, D. L. A. Tjaden, and J. W. F. Dorleijn, "Calculation of the Stray Field of a Magnetic Bubble, with Application to Some Bubble Problems," Philips Res. Repts. 27, 7 (1972).

[20] T. Kobayashi, D. M. Heinz, E. C. Whitcomb, P. J. Besser, and J. L. Archer, "Self-Biased Structures for Bubble Devices," 1977 Intermag Conf., paper 33-7, Los Angeles, June, 1977.

[21] Y. Hidaka, K. Yoshimi, T. Hibiya, and M. Mikami, "Improved Propagation Margin in YIG Coated LPE Garnet Films for Bubble Devices," AIP Conf. Proc. 24, 633 (1974).

$h_o \ll h_1$ and h_2. Then, we have only to add this field to the others in Eq (1)-(3). This field is given, respectively, by

$$\text{Single:} \quad \overline{H}_{02} = -\frac{M_o}{2M_2}\left(\frac{h_o}{h_2}\right)\ell_n \left[\sqrt{\left(\frac{2h_2}{d_2}\right)^2 + 1} + \left(\frac{2h_2}{d_2}\right)\right]$$

$$\text{Double:} \quad \overline{H}_{oi} = -\frac{M_o}{2M_i}\left(\frac{h_o}{h_i}\right)\ell_n \left[\sqrt{\left(\frac{2h_i}{D_i}\right)^2 + 1} + \left(\frac{2h_i}{D_i}\right)\right]$$

where M_o is the saturation magnetization of the intermediate layer. Thus the stability equations can be solved approximately for the type 3 structure.

The type 4 structure is even more difficult to analyze. The reason is that because of direct exchange coupling the double bubble wall will be pinched, as shown in Figure 4(a), if $D_1 < D_2$. The diameter tapering will take place mostly in layer 2 where the wall energy is lower. A rigorous approach to analyzing this structure is
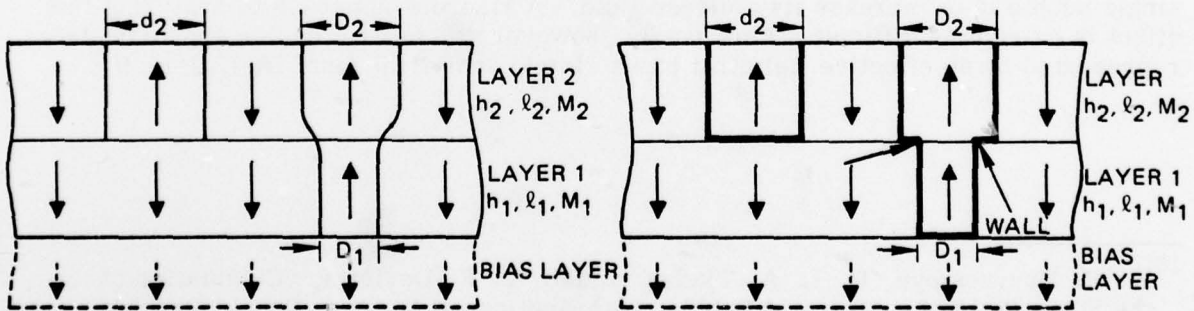

Figure 4a.   Schematic of Type 4
Domain Structures

Figure 4b.   Model for Type 4
Domain Structures

20

thus extremely difficult and a simple model has to be developed to represent the structure. We tentatively propose a model in which the tapered wall is represented by a horizontal wall with its energy equal to σ_{w2}. The model structure is illustrated in Figure 4. Then, since the additional wall energy is $\pi\sigma_{w2}(D_2^2 - D_1^2)/4$, it adds to Eq (2) and (3) the effective fields, $\overline{H}_2$ and $\overline{H}_1$, respectively, which are given by

$$H_i = (-1)^i \frac{\ell_2}{2h_i} \qquad (i = 1, 2) \tag{4}$$

and Eq (2) and (3) must be solved with $\ell im\ h_0 \to o$. Incidentally, the single bubble presents no problem since it is identical with that in the type 2 structure, and can readily be analyzed by Eq (1).

3.4 EXAMPLE CALCULATIONS

Now let us take the type 2 structure as an example and see how the material parameters can be tuned to specific values to meet specific device requirements. The type 2 structure is schematically shown in Figure 5 for the lattice region and the input/output (I/O) region. For simplicity, layers 1 and 2 are assumed to be made of the same material, i.e., $\ell_1 = \ell_2 = \ell$, $M_1 = M_2 = M_S$, and $q_1 = q_2 = q$. Let us look at the lattice region first. Note here that the single bubble is "single-biased" and the double bubble is "double-biased" as seen from the schematic illustration of the
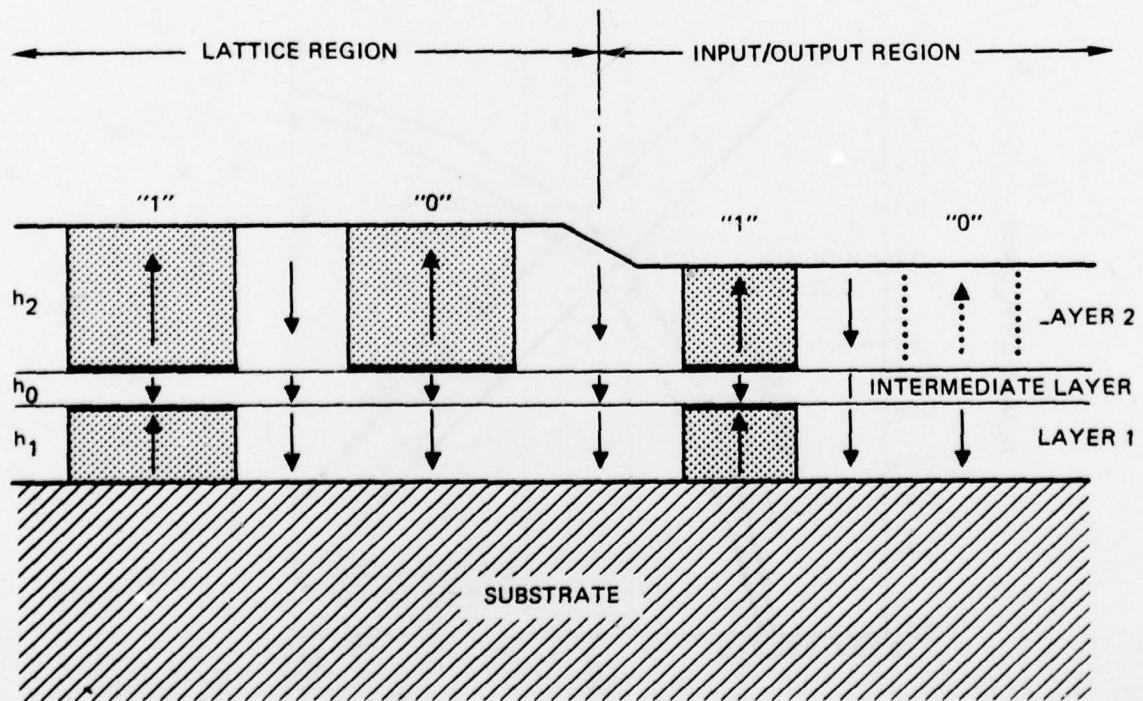

Figure 5. Double Bubble Configuration of a MMDLF (Type 2 Structure)

capping walls in Figure 5 (thick lines). It can be shown that the analysis described previously that the normalized effective bias field for the single and the double bubbles are given respectively by the following:

$$\frac{H_{eff}}{4\pi M_s} = \begin{cases} \dfrac{\ell}{2h_2} \left(1 - \dfrac{p}{q}\right)^{1/2} & \text{(single)} \\[3ex] \dfrac{\ell}{h^*} \left(1 - \dfrac{1}{q}\right)^{1/2} & \text{(double)} \end{cases} \tag{5}$$

where h^* is the effective thickness of the double bubble. Equation (5) is plotted with $q = 5$ in Figure 6 as a function of h/ℓ (h_2/ℓ for the single bubble and h^*/ℓ for the double bubble). Also plotted in Figure 6 are the bubble collapse field, H_0, and the run-out field, H_2, vs. h/ℓ.

Now, suppose values for h_o, h_1, and h_2 are chosen such that the stability points for the single and double bubbles correspond, respectively, to points A and B in the stability chart. These points are slightly below the run-out line. Thus, if the single and double bubbles are isolated, they will strip out. It can be shown, however, that if they are closely packed together, they form a uniform bubble lattice.
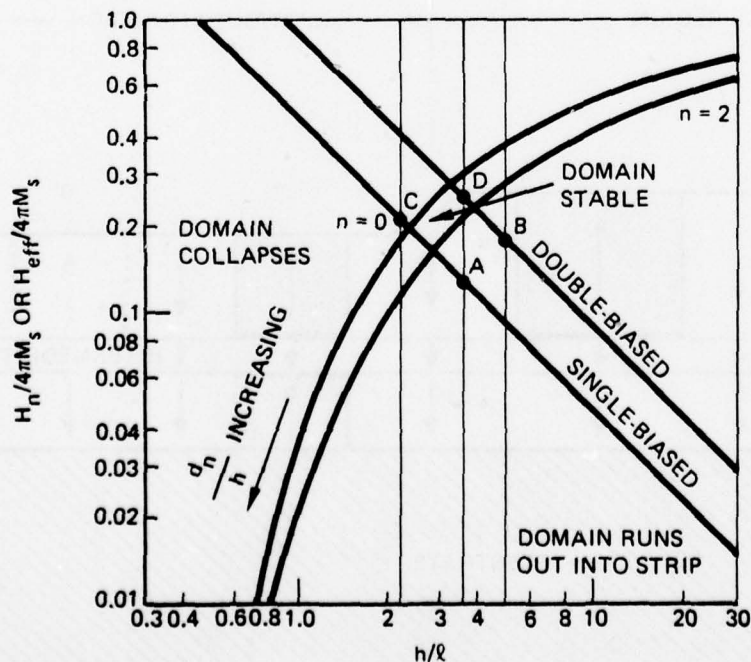

Figure 6. Stability Conditions for Single and Double Bubbles

22

Turning to the I/O region in Figure 5, suppose the thickness of layer 2 is reduced in the I/O region so that the stability points of the single and double bubbles move up along the self-bias lines from points A and B to points C and D, respectively. Point C passed the stable region and moved into the collapse region, whereas point B moved right into the stable region. Thus, if an accessed column of information carrying bubbles is driven into the I/O region across the thickness ramp, single bubbles would spontaneously collapse and double bubbles would be stable without an external bias field. In other words, a double/single bubble pattern can be automatically converted to a bubble/no bubble pattern. The stable double bubbles can then be led into a conventional field access detector circuit.

The next three figures show quantitatively how the above properties can be realized. Plotted in the figures are the diameters (defined in Figure 3) of the single and double bubbles in the lattice and I/O regions as a function of the external bias field. All the dimensions are normalized with respect to ℓ_2, the characteristic length of layer 2, and the bias field with respect to $4\pi M_2$, the spontaneous magnetic induction of layer 2. Figure 7 shows the case where the intermediate layer is rather thick ($h_0 = h_1$). It is seen that D_2 and d_2 in the lattice region are fairly close to each other. (D_2 is $\sim 10\%$ greater than d_2.) Indeed, in the I/O region, the double bubble is fully self-biased, i.e., the midpoint of the stability range falls on the zero bias, whereas the single bubble is far into the negative bias region, i.e., it collapses at the zero bias. D_2 and d_2 are even more closer to each other for the case where the layer 1 is thinner and the intermediate layer is extremely thin. This is shown in Figure 8. As in the first case, the double bubble is stable but the single bubble is not at the
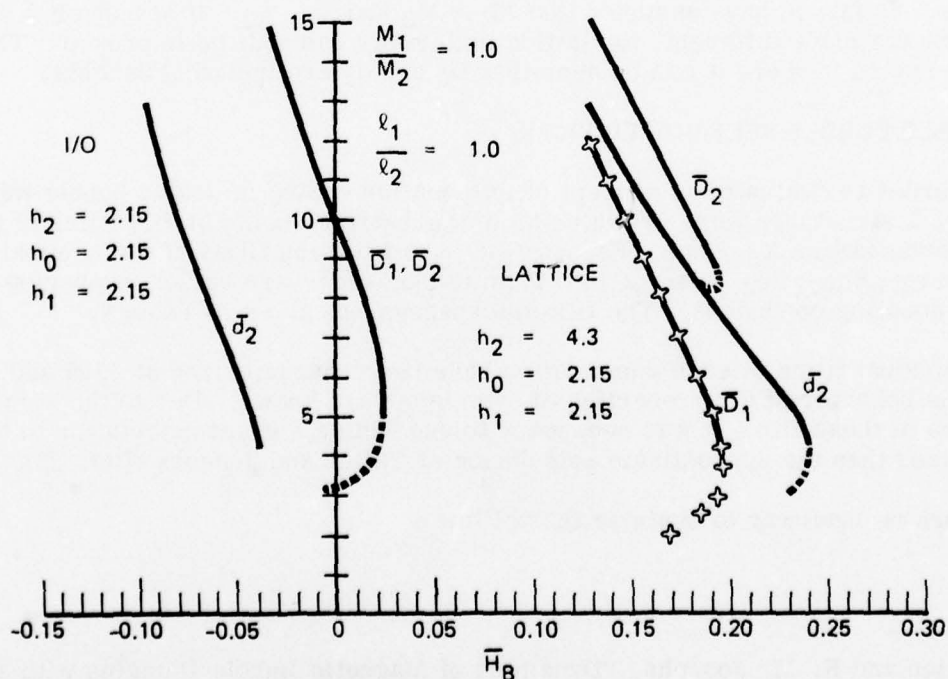

Figure 7. Diameters of Single and Double Bubbles for the Case Where the Intermediate Layer is Thick
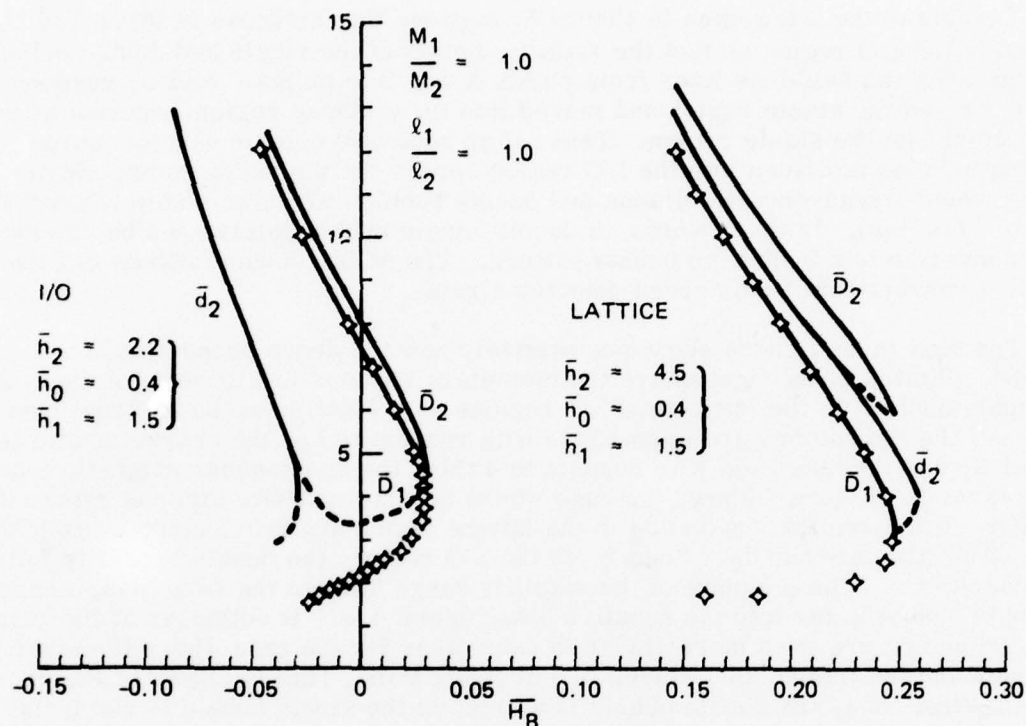
23

Figure 8. Diameters of Single and Double Bubbles for the Case Where the Intermediate Layer is Thin

zero bias. So far we have assumed that $M_1 = M_2$ and $\ell_1 = \ell_2$. If M and/or ℓ of the two layers are made different, the lattice uniformity can still be improved. This is shown in Figure 9 where it can be seen that D_2 and d_2 are indistinguishable.

3.5 DOUBLE BUBBLE SELF-BIASED FILMS

In order to evaluate the concept of information coding in double bubble wafers, three type 2 structures were grown on 25 mm substrates using bubble films of the nominal composition $Y_{2.6}Sm_{0.4}Fe_{3.8}Ga_{12}O_{12}$ and biasing films of the nominal composition $Er_{2.2}Eu_{0.8}Fe_{4.2}Ga_{0.8}O_{12}$. Film thicknesses were varied to provide a range of coupling conditions. The film thicknesses are given in Table 4.

Individual films of each composition have been characterized at 0, 25 and 50°C so that the behavior of the properties of each layer are known. Due to the small h/ℓ values of these films it was necessary to use Thiele's exact calculation to obtain $4\pi M_s$ rather than the approximate calculation of Callen and Josephs (Ref. 22).

Work is underway to evaluate these films.

---

[22] H. Callen and R. M. Josephs, "Dynamics of Magnetic Bubble Domains with an Application of Wall Mobilities," J. Appl. Phys. 42, 1977 (1971).
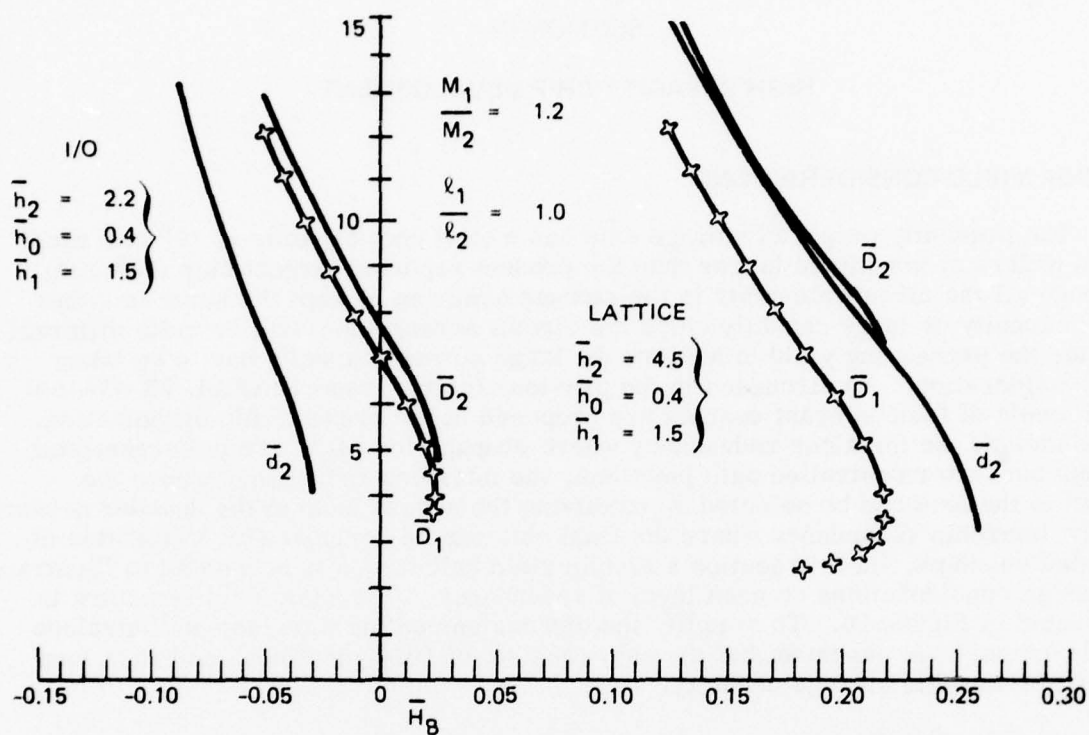
24

Figure 9.   Diameters of Single and Double Bubbles for the Case Where the Magnetizations in Layer 1 and 2 are not Equal

TABLE 4.   FILM THCKNESSES OF DOUBLE BUBBLE SELF-BIASED FILMS

Designation	h_1^* μm	h_0^* μm	h_2^* μm
M36	1.15	0.31	1.49
M41	0.89	0.36	1.46
M43	0.67	0.41	1.38
* Films 1 and 2 are $Y_{2.6}Sm_{0.4}Fe_{3.8}Ga_{1.2}O_{12}$			
† Film 0 is $Er_{2.2}Eu_{0.8}Fe_{4.2}Ga_{0.8}O_{12}$			

25

SECTION IV

HIGH CAPACITY CHIP DEVELOPMENT

4.1 CHIP YIELD CONSIDERATIONS

The presently proposed storage chip has a total chip capacity of 10^8 bits which is two orders of magnitude larger than the present reported largest chip (10^6 bits) Although all the circuit elements in the storage area can be kept the same in either small capacity or large capacity chips the circuit arrangement will be quite different because the processing yield to achieve the large storage capacity has to be taken into consideration. As discussed in the previous interim report (AFAL TR-77-198) three levels of fault tolerant designs are proposed in the present chip organization. These include the intraloop redundancy where propagation paths are interconnected through conductor controlled path junctions, the interloop redundancy where the access to the loop can be selected by modifying the access code in the decoder network and the interchip redundancy where the final chip can be composed by a selection of operated subchips. In this section a simple yield calculation is presented to illustrate the design considerations on each level of redundancy. The basic chip structure is illustrated in Figure 10. To simplify the discussions on the interloop and intraloop redundancies, it is assumed that the chip consists of 1024 good loops and each loop has 10^5 bits usable storage capacity.

4.1.1 Modification Yield

The most critical factor in the design of the on-chip correction fault-tolerant circuit is the circuit modification yield, Y_m. A nonunity modification yield will limit the effectiveness of the redundancy design and ultimately limit the maximum storage capacity that can be achieved in a single chip. The fault tolerant circuit designs proposed in the previous interim report (AFAL TR-77-198) emphasize that all the onchip correction will be done on the conductor level only. The process involved is simply to open circuit a conductor line. This process can be achieved by using laser scribing or selective etching on the conductor patterns. The correction area can also be designed such that it is far away from the propagation paths thus relaxes the alignment and resolution requirements. The circuit designs are also arranged that the number of corrections required in the chip equals to the number of redundancies in the design. Thus the total modification lost can be kept to a minimum.

A test circuit for evaluating the concept of modifying conductor leads is incorporated in the 1088 test chip. As shown in Figure 11, an exchange switch is arranged such that the active switch conductor is shorted by a by-passing conductor. Using laser pulse bombardment, the conductor can be opened to actuate the switch as suggested in the previous report. The laser beam can be aligned to a few microns in diameter without any difficulty. The burring of the conductor is a straight-forward process. The damaged area examined under normal operating magnetic fields does not cause any spontaneous nucleation. Thus in the following analysis, it is assumed that the correction yield Y_m is equal to one and the effect of the correction process is ignored.
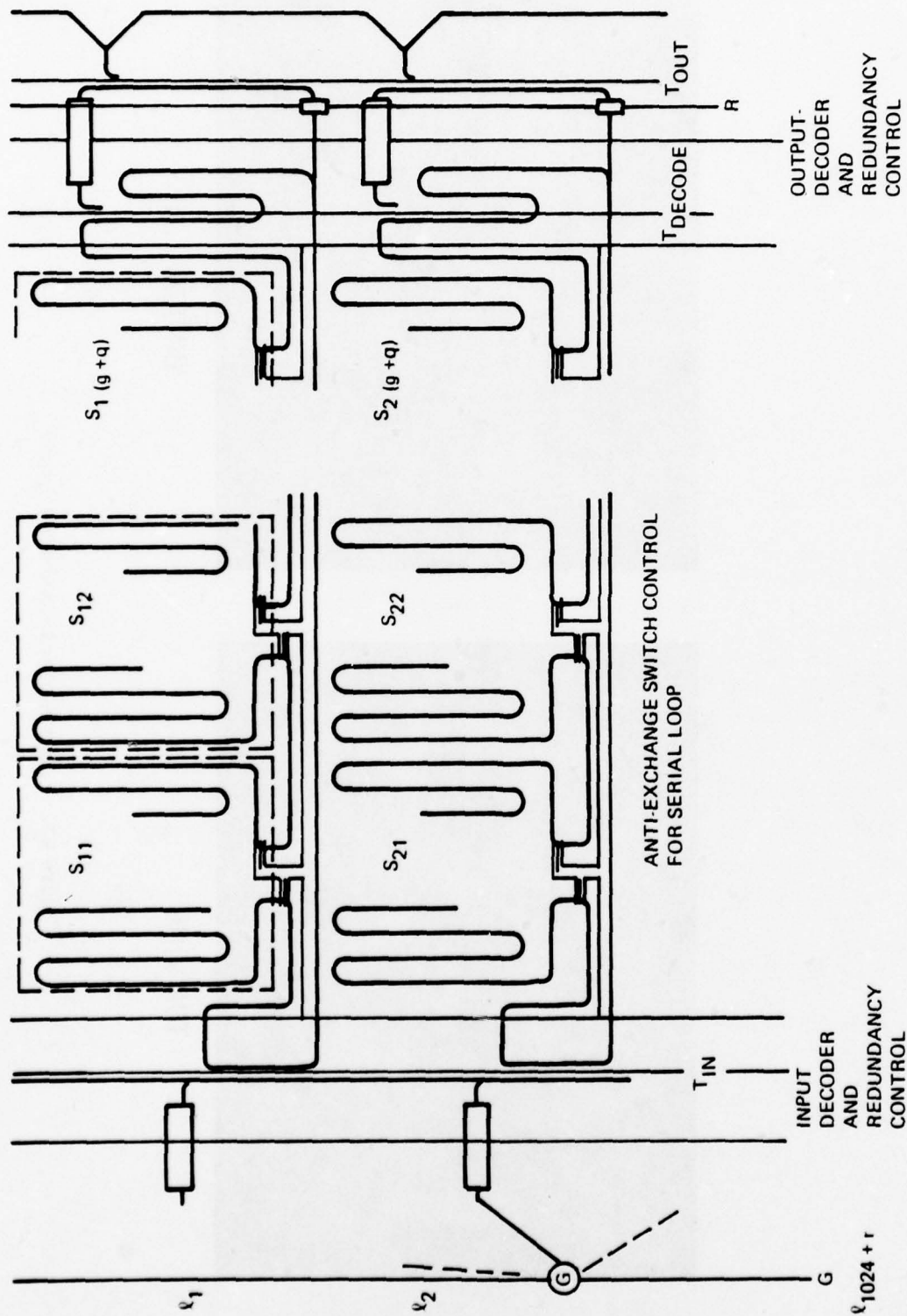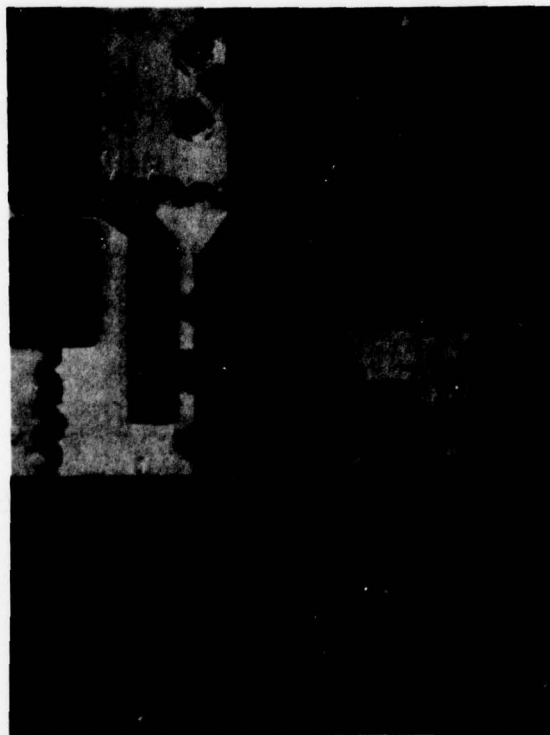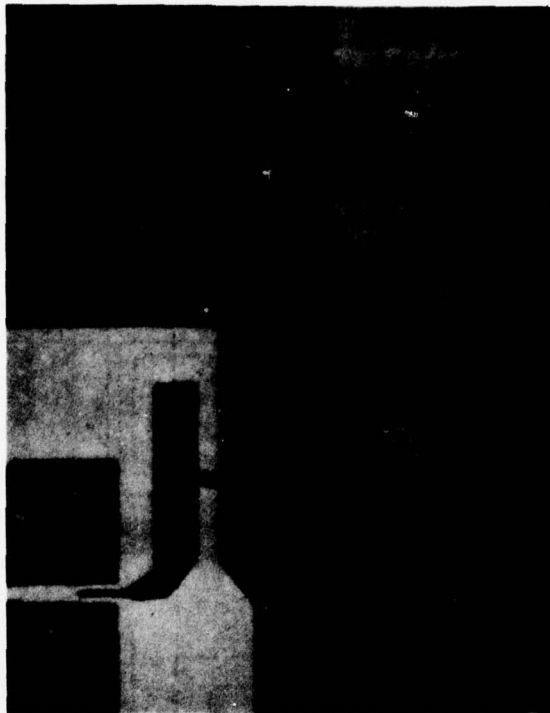
Figure 10. Storage Loop With Redundant Paths

27

BOTTOM VIEW

TOP VIEW

Figure 11.   Laser Scribed Conductor Leads

4.1.2 Interloop Redundancy

As shown in Figure 10, the total number of loops in the chip is assumed to be 1024+r where r is the number of redundant loops. Each loop has a processing yield of Y_ℓ and the total chip yield Y_C is then

$$Y_c = \sum_{i=1024}^{1024+r} \binom{1024+r}{i} \; Y_\ell^i \, (1-Y_\ell)^{1024+r-i}$$

$$= I_{Y_\ell} \, (1024, \; r+1)$$

(6)

Here the yield of the common I/O area is temporarily ignored because it is relatively small as compared to the storage area.

Eq (6) represents the probability of finding at least 1024 good loops in 1024+r loops when the probability of each loop being good is Y_ℓ. This Eq can be related to the F-(variance ratio) distribution through

$$Q(F/\upsilon_1, \; \upsilon_2) = I_x(\nu_1/2, \; \nu_2/2), x = \frac{1/2}{\upsilon_2 + \upsilon_1 F}$$

(7)

Using the tabulated F-distribution values the required loop yield Y_ℓ as a function of precentage redundancy for a given chip yield can be estimated as shown in Figure 12. Under fixed chip yield conditions, the required loop yield decreases as the precentage redundancy increases. For example, to achieve 50 percent processing yield, $Y_C = 0.5$, with 10 percent redundancy (or $r = 102$), the loop yield has to be better than 0.91. However, if the redundancy is increased to 100 percent or $r = 1024$, the loop yield can be dropped to 50 percent.

In this analysis, the subdivision of the chip is not considered. r redundant loops are shared among the 1024 loops. In the hybrid chip design, the chip will be separated into M subchips with 1024/M good loops in each subchip. The number of redundant loops for each subchip is also reduced by a factor of M. The efficiency of the redundancy will be lowered because the redundant loop in one subchip cannot be shared by other subchips.
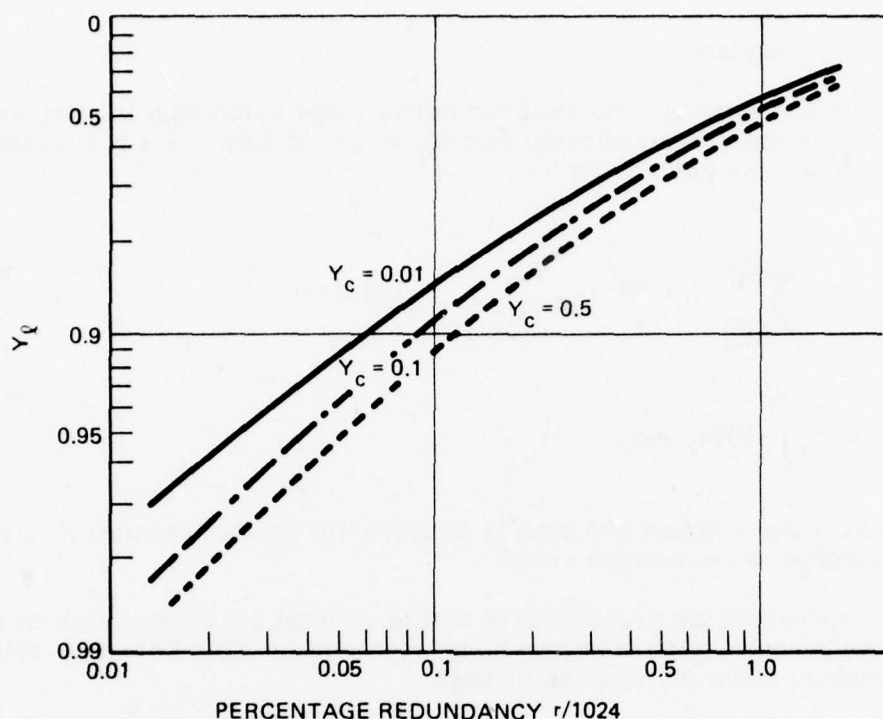
29

Figure 12. Loop Yield as a Function of Redundancy
Under Fixed Chip Yield

4.1.3 Intraloop Redundancy

The loop yield again is a function of the amount of redundancy put inside the loop or the number of separable sections in the loop. Assuming a section yield of Y_S, the loop yield Y_ℓ can be given by

$$Y_\ell = \sum_{i=g}^{g+q} \binom{g+q}{i} Y_S^i (1-Y_S)^{g+q-i} \tag{8}$$

$$= I_{Y_S} (g+q, q+1)$$

The required Y_S for a specified Y_ℓ value again is a function of the redundancy within the loop. Figure 13 plots Y_S vs percentage of redundancy or q/g for $Y_\ell = 0.9$ and $Y_\ell = 0.99$ cases. The requirement on section yield relaxes as the redundancy percentage increases.

The other parameter involved in the loop yield is the number of sections. For a fixed redundancy percentage, Y_S can be relaxed by increasing the number of
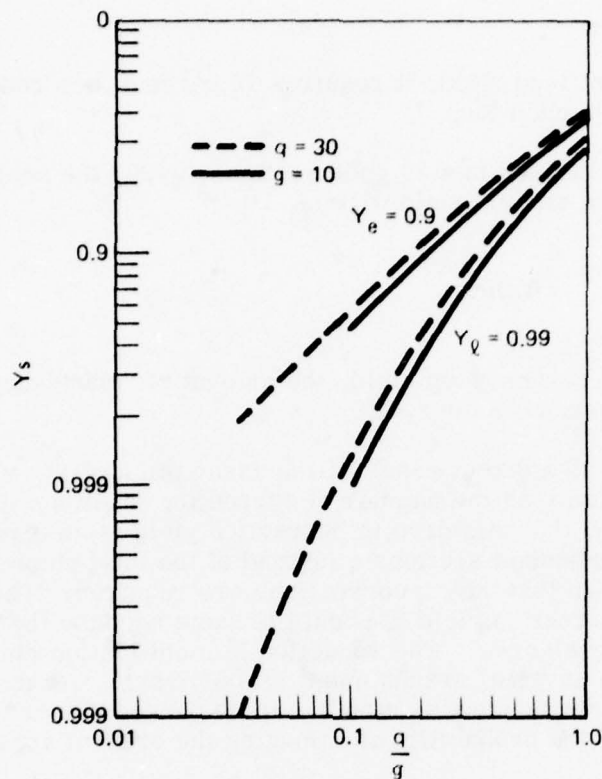
30

Figure 13. Required Section Yield as a Function of Redundancy in the Loop

sections in the loop. Of course, here we assume that there is no complication due to on-chip modification yield. If this yield is not one, then the number of sections cannot be arbitrarily increased.

The section yield is a function of the processing defect density. Defects may occur in the garnet and in the circuit overlay. The yield can be approximated by

$$Y_s = e^{-n_g A_g} e^{-n_p A_p}$$

where n_g and n_p are the defect density for garnet and permalloy and A_g and A_p are the effective garnet and permalloy area for the section respectively. The numbers obtained from present yield model are $n_g \sim 4/cm^2$ and $n_p \sim 64/cm^2$ for a 4 μm circuit. If we assume a section capacity of 10^4 bits (g=10) with 4 μm period circuits, and assume $A_g = A_p = A_s$

$$Y_s \sim e^{-(n_g + n_p)A_s}$$

$$= e^{-68 \times 10^4 \, (4 \times 10^{-4})^2}$$

$$= 0.90$$

31

To achieve a 90 percent loop yield, it requires 20 percent loop redundancy or there should be 12 sections in each loop.

If the loop is subdivided into 30 good sections, g=30, the section area is reduced by 1/3, and the section yield will be

$$Y_s = (0.9)^{1/3} = 0.966$$

For the same 90 percent loop yield, the amount of redundancy can be reduced to 6 percent or 2 redundant sections.

Apparently, this is a direct result of the assumption of $Y_m = 1$. In reality, Y_m will deviate from unity as the number of correction junctions increases. However, it should be noted that this drop in correction yield is an exponential function of the number of the redundant sections q instead of the total number of sections g+q. This is due to our design that only q corrections are required. Therefore, in the above example, the correction yield is about the same because there are only two redundant sections in each case. The reduction in modification yield as g increases is primarily due to the physical arrangement in the circuit. As the number of sections increases, the conductor section has to be packed closer to the propagation circuit thus increasing the probability of damaging the critical area in the correcting process.

4.1.4 Interchip Redundancy

Since the proposed hybrid decoder chip is organized in M identical subchips, it would be possible to process each subchip separately and then assemble the whole chip in the final package by interconnecting all the control leads. If each subchip has a processing yield of Y_{sc}, the yield for the total chip processed as one chip is

$$Y_c = Y_{sc}{}^M$$

However, if each subchip is separately processed and tested, the yield for the assembled chip will be

$$Y_c = Y_{sc} \cdot Y_h{}^M$$

where Y_h is the yield for handling and assembling the subchips.

Normally, Y_h can be close to 1 for a properly structured subchip. However, additional cost will be added to the chip area, processing, handling and packaging. This approach also increases the number of bubble memory parts in the system and thus may degrade the system reliability. The final selection would depend on the final subchip yield. If possible, this type of subdivision should be avoided.

4.1.5 Impact on the Chip Layout

In the calculation of intraloop redundancy, only the yield of the storage sections is considered. The yield of the bubble path which interconnect these sections is ignored. This assumption is only justified when the total area of these propagation paths is much smaller than that of each storage section. The actual area then depends critically on the actual circuit layout. Two possible chip organizations are illustrated in Figure 14. In (a) the chip is arranged such that input and output areas are concentrated at two opposite edges. In this arrangement the overhead I/O area can be kept minimum. Unfortunately, each storage loop has to be spread across the whole chip and the redundancy arrangement proposed in Figure 10 would be very difficult to achieve. This is because the interconnecting paths and switch junctions may occupy more area than the storage sections. The calculated yield would be much smaller than that predicted in Figure 12. The other alternative is to subdivide the chip in two directions as shown in Figure 14 (b). In this manner the area ratio between connecting path and storage section can be close to ideal value. However, the number of I/O ports has to be increased reducing the total storage efficiency. In this arrangement, the chip size is effectively reduced for smaller subchips. The final choice of the optimum organization would be determined by the projected circuit yield.
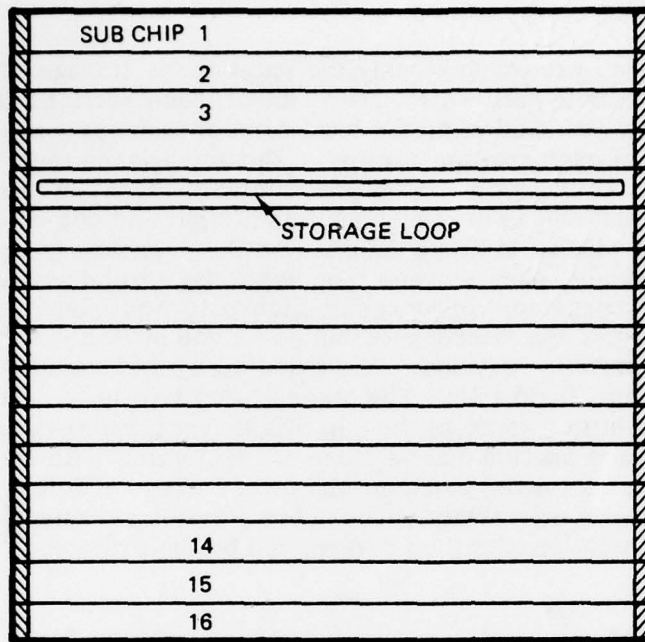
4.2 M1088 TEST CHIP EVALUATION

The test chip 1088 described in last interim report (AFAL TR-77-198) was evaluated further in this reporting period. The circuit layout is shown in Figure 15 with key components numbered. A brief evaluation was first made on the overall chip performance and then the study concentrated on the retarding switch design. This section will describe the overall chip evaluation and next section will show the detail study on the retarding switch.
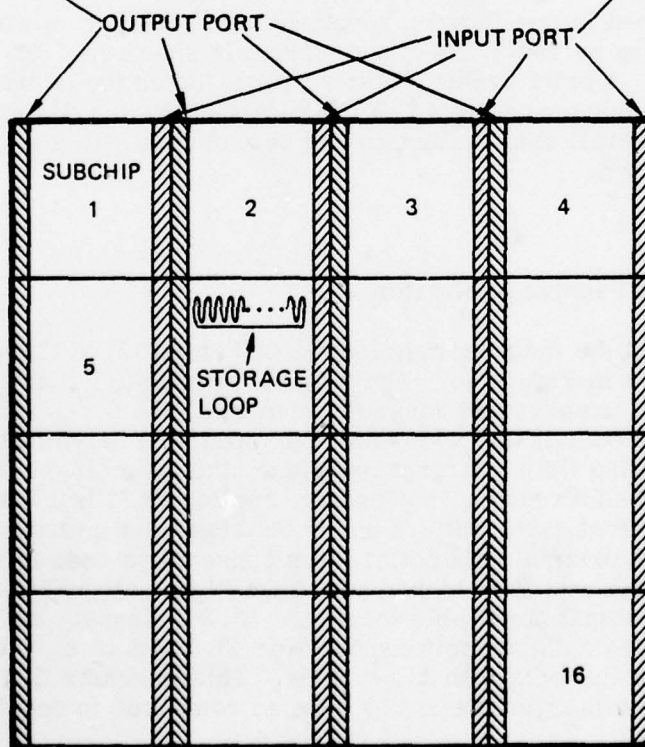
4.2.1 Overall Chip Evaluation

a. Main Storage Loop and Passive Replicator

The propagation margins of the main storage loop (1 in Figure 15) at three different temperatures are shown in Figure 16. The reliable propagation bias margin is about 8 to 10 Oe in the temperature range between 20°C and 60°C. This is less than 50 percent of the expected half disk element. The minimum drive field is also high especially at 20°C. Using field interrupt technique, the anomality in this measurement is found to be related directly to the passive replicator (2 in Figure 15) as shown in Figure 17 (a). A typical error pattern under the bias field interrupt is illustrated in Figure 17 (b). The original data pattern was consecutive ones in words 43 and 44. (8-bit word). The chip was first biased at 123 Oe (H_{ZO} + ΔH_Z = 111.5 Oe + 1.5 Oe). After 10 to 20 bias pulses, the bubble located at 43.3 collapse. As the bias field increases, more bubbles collapse between location 43.0 and 43.6. However, no bubble in word 44 collapses even with ΔH_Z = 6 Oe. This indicates that the passive replicator lowers the bias margin at least by 6 Oe as compared to regular half disk circuit.

Apparently, using the wide spread in the passive replicator output port with multiple bubble "cutter" bars does not help the bubble replicating function at all. Instead, the large separation between the main path and the replicated path requires

33

Figure 14. Possible Chip Subdivisions

Figure 15. Test Chip 1088

M1088 CHIP NO. 2
TOTAL REGISTER

$20^{\circ} \pm 1^{\circ}C$

$40 \pm 1^{\circ}C$

$60 \pm 1^{\circ}C$
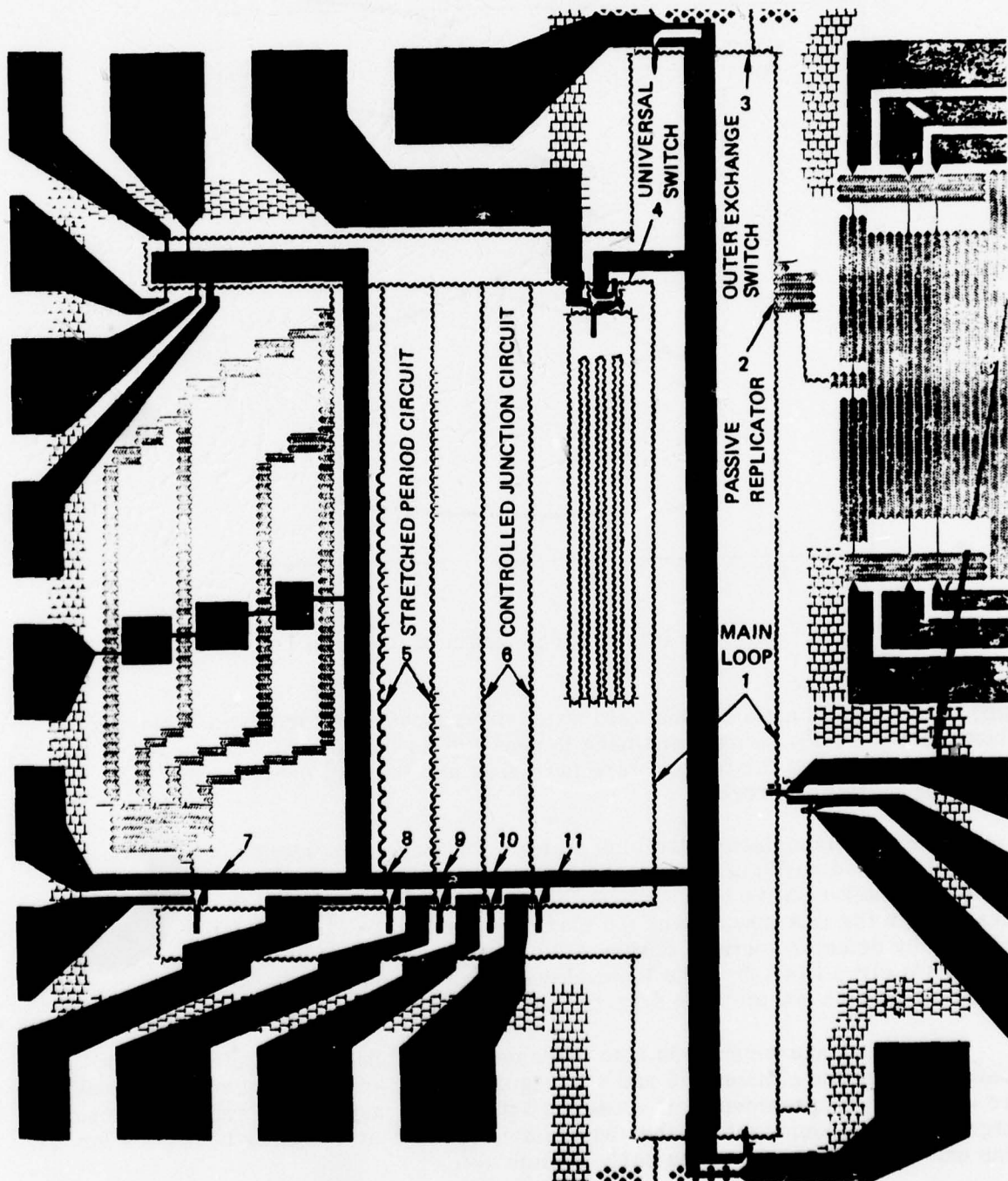
δH_{BIAS} (Oe)

12
10
8
6
4
2
0
-2
-4
-6
-8
-10
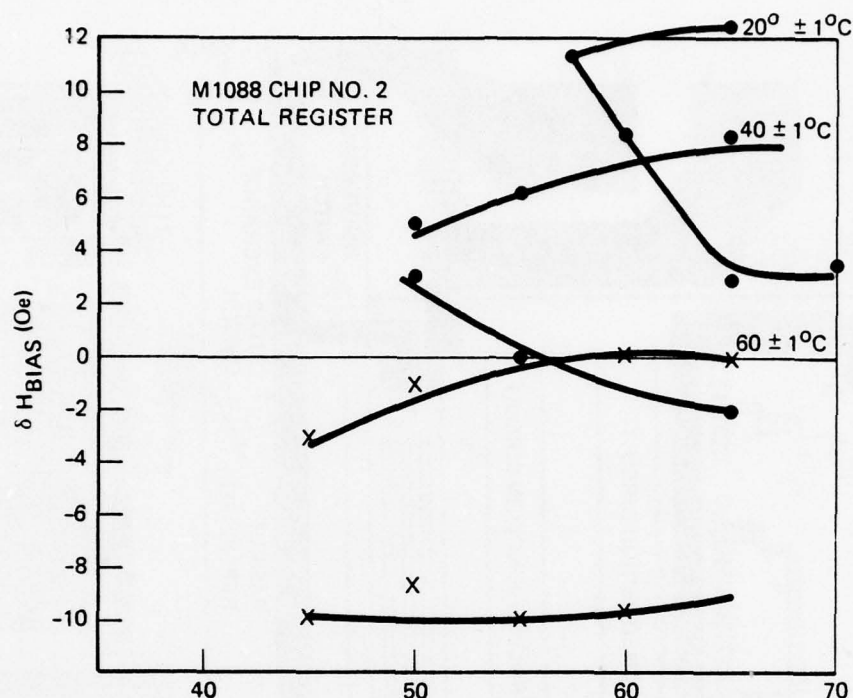
40   50   60   70

Figure 16.   Propagation Margin of the Main Loop

large driving field and low bias field which are responsible for the poor margin shown in Figure 16.   This phenomena is sensitive to the domain wall energy of the material because as the temperature increases and the wall energy drops the operating margin improves.

A brief comparison of the bias margin was made on a section of the propagation track illustrated on Figure 18 which shows the various components in this selected track with their relative bit locations in 8-bit word.   Figure 19 shows the relative bias margin for this track.   The top margin is limited by the replicator (43.3) followed by detector section, corner (47.4) and outer exchange switch merge (3 in Figure 15) circuit (47.7).   The low end margin is limited by the half disk to chevron transition circuit (44.0).   The straight line half disk circuit margin is about 25 Oe.

Margin measurement was also made on the stretched period elements and controlled junction elements (5 and 6 in Figure 15) shown in Figure 20.   The results are generally in agreement with those reported in the last interim report.   Those large period elements with pusher bar located at the center usually have poor low bias end margin because of the early stretch out.
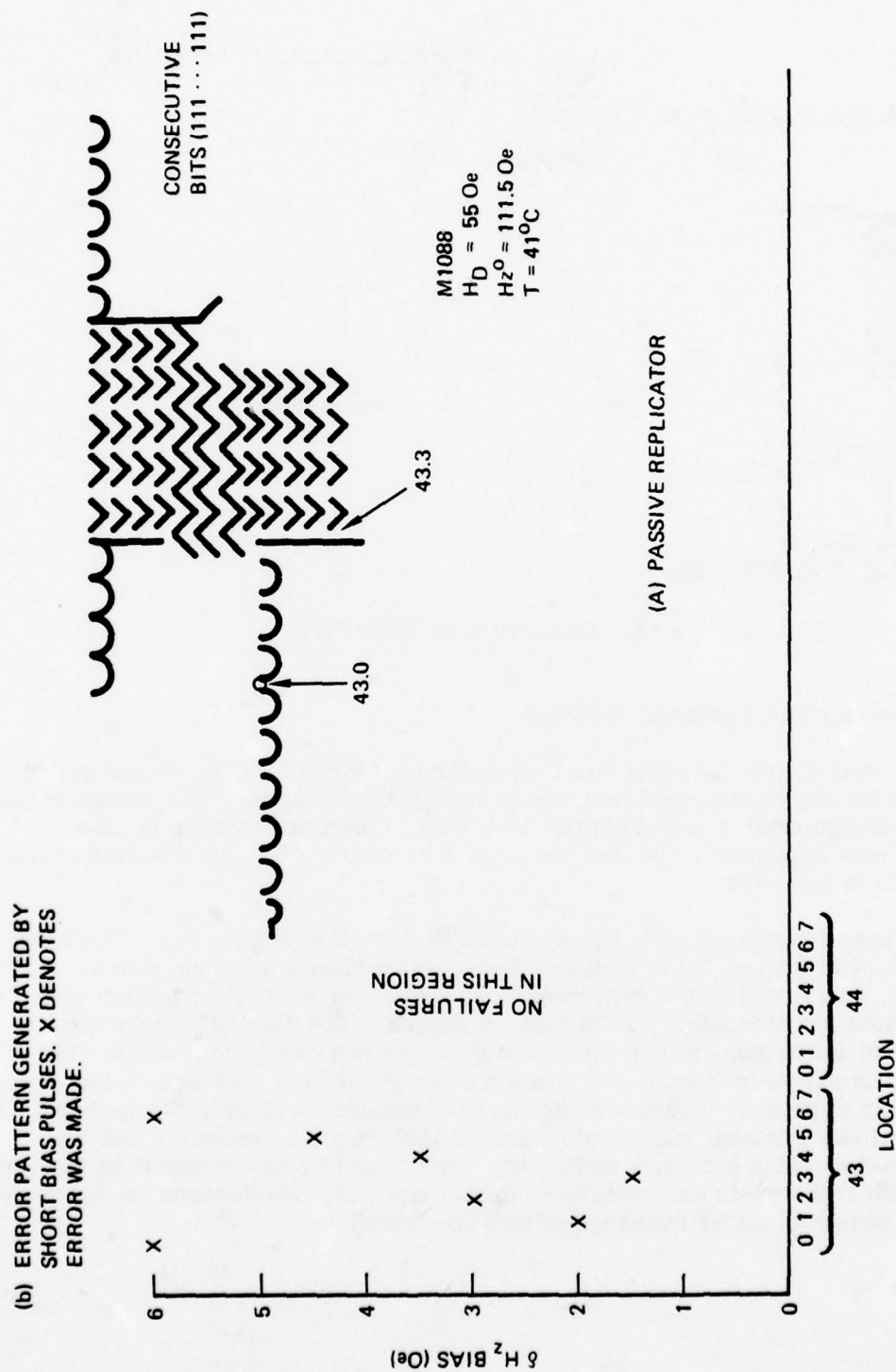
Figure 17. Passive Replication Design and Associated Error Scan Pattern
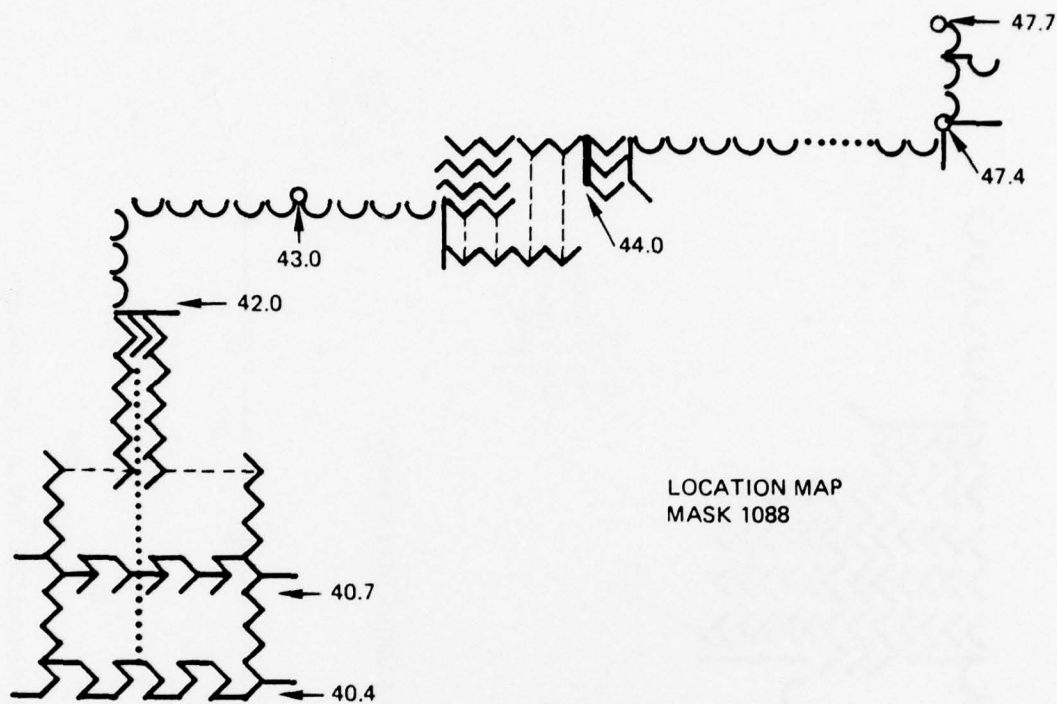
LOCATION MAP
MASK 1088

Figure 18. Location Map Mask 1088

b. Transfer and Exchange Switches

As shown in Figure 15 there are 5 transfer switches (7, 8, 9, 10 and 11) in this test chip for interconnection test tracks with the main loop. This design is the same as the design used in major-minor loop chip. The performance is also identical to those reported in the major-minor loop chips. Thus no detailed evaluation was made in this chip.

Two types of exchange switches are used in this chip (Figure 21). The universal switch (4 in Figure 15) is connected to a small closed test loop which, unfortunately, has very limited operating margin because of its propagation structure. Thus this switch function could not be fully evaluated. The outer exchange switch (3 in Figure 15) interconnects the main storage loops in two adjacent cells. The phase margin is shown in Figure 22.   The transfer out switch ("go away") has a wide-margin similar to regular transfer switch. The transfer-in switch ("come back") margin is limited, probably due to misalignment between the conductor and the permalloy masks. This exchange switch has been tested by interconnecting the conductors in both transfer-in and transfer-out sections. No interference on the switch function was observed under exchange switch operation.
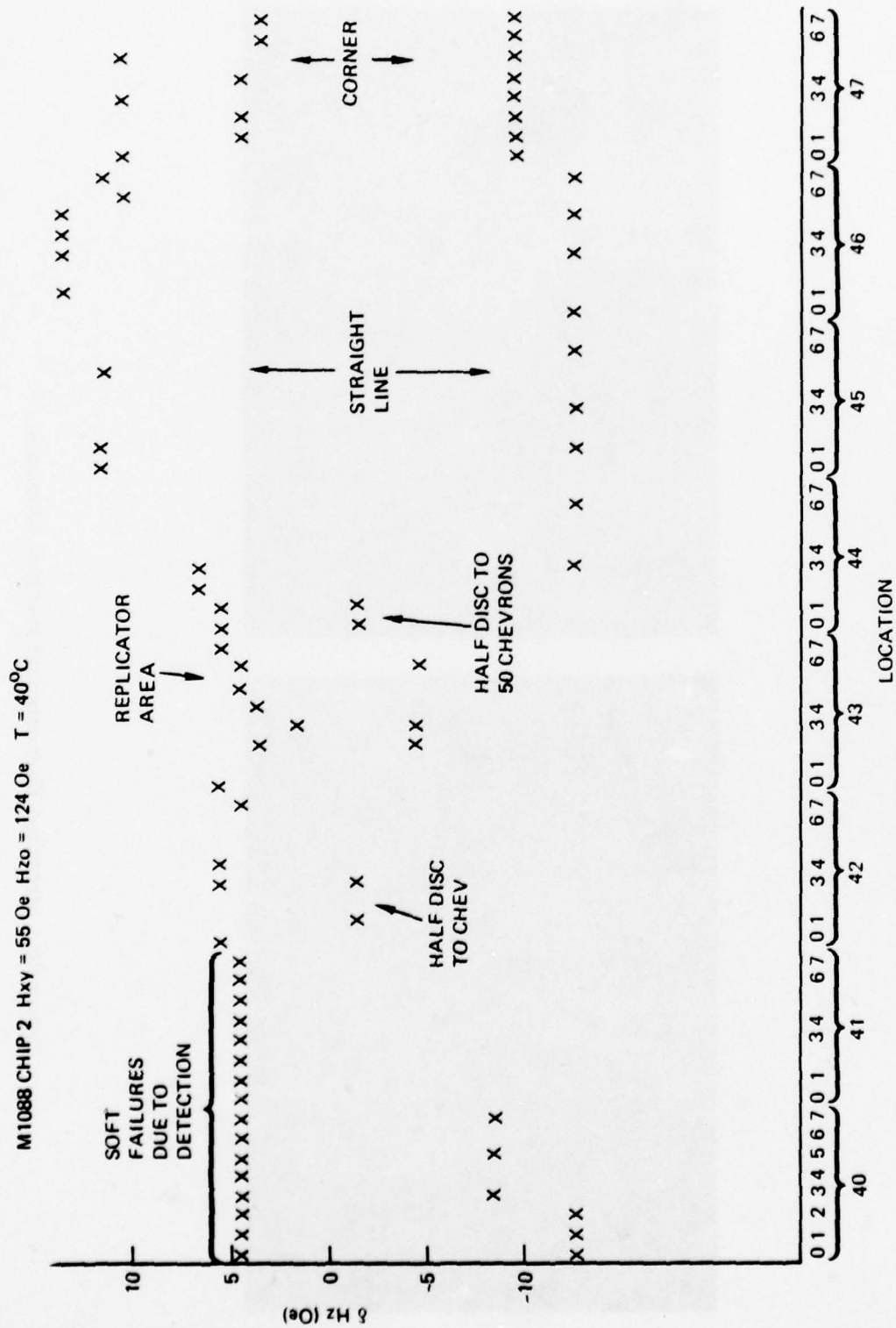
38

Figure 19. Bias Margin of Various Components in the Selected Section Shown in Figure 18.
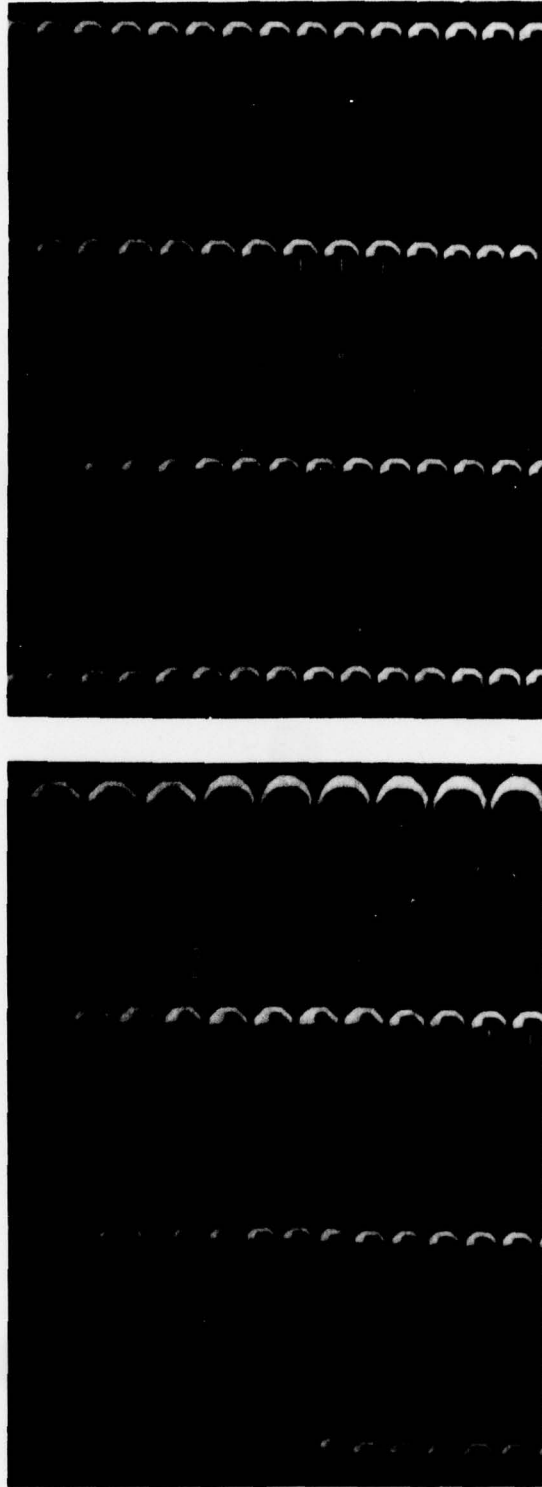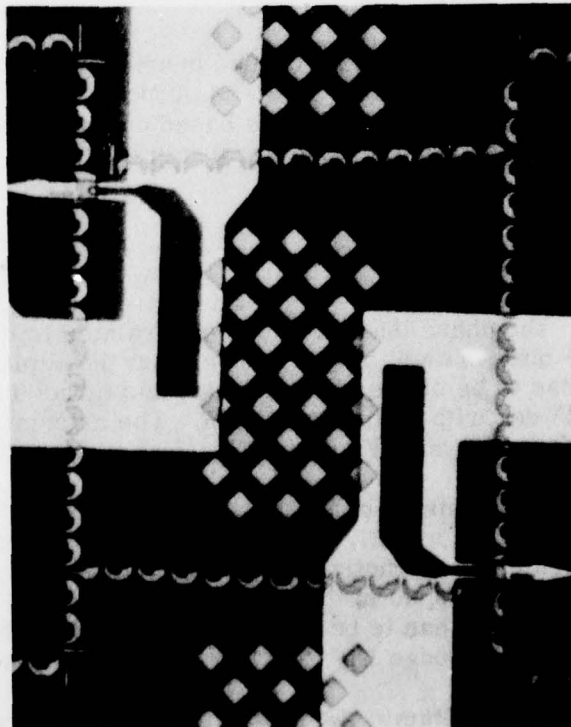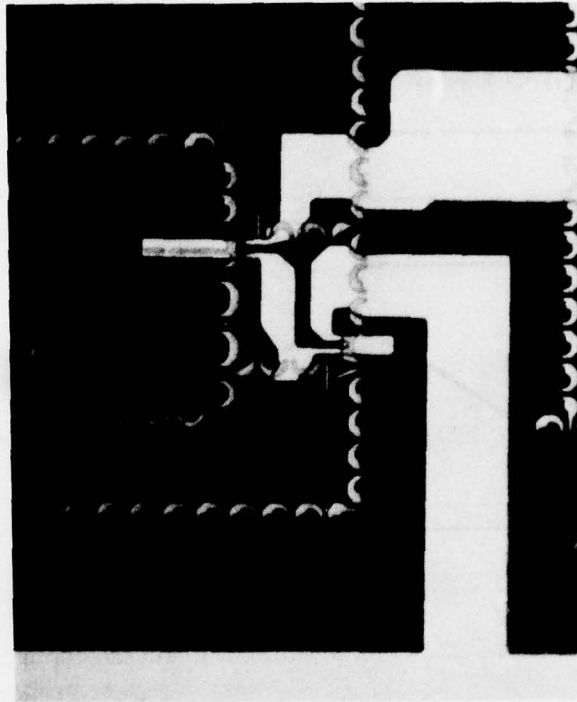
Figure 20. Stretched Elements and Junction Elements

40

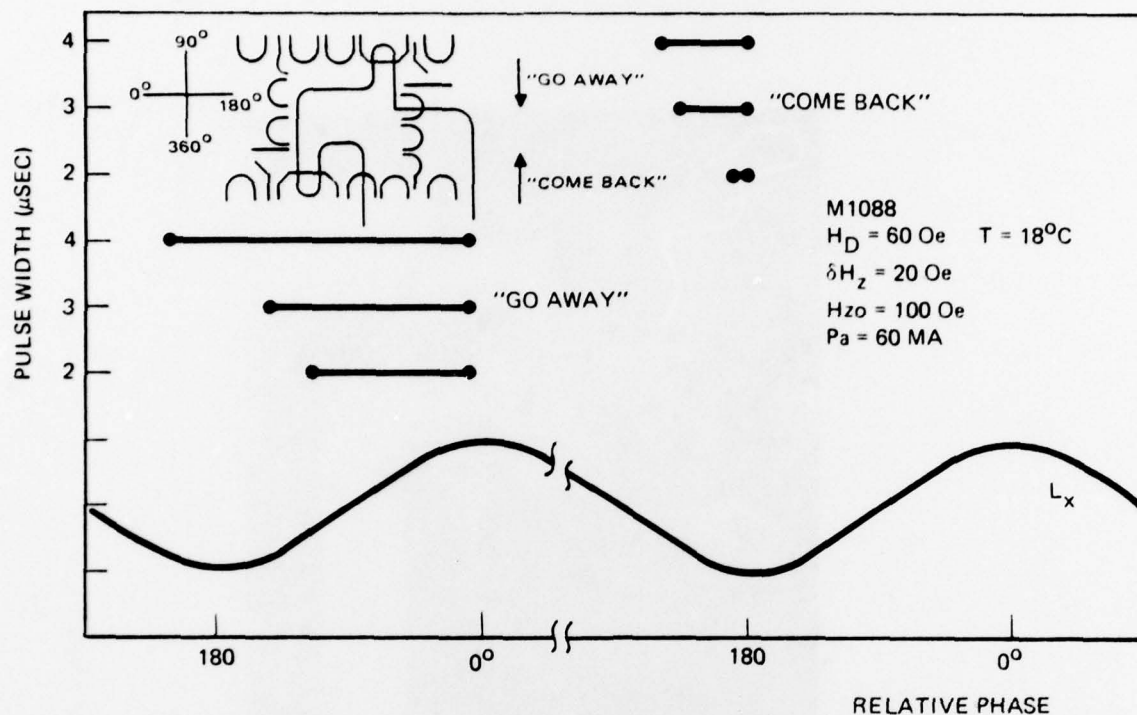Figure 21. Exchange Switch and Universal Switch

41

Figure 22. Phase Margin of the Exchange Switch

4.2.2 Retarding Switch Evaluation

One of the key elements in the proposed hybrid decoder chip is the retarding switch. The first workable switch design was proposed on T-bar circuit (Ref. 23). Variations on half disk propagation circuits based on the same design principle have been studied in the 1088 test chip. The circuit arrangements are illustrated in Figure 23.

The operating of this retarding switch can be understood by studying the phase margin of the swtich control pulse. Figure 24 shows the range of the phase margin for three different pulse widths for successful retarding operation on the switch design, Figure 23. The phase margin is directly related to the pulse width used. By comparing these margin data, it can be seen that the limitation on the pulse condition is that it has to be started before 0 deg and turned off after 45 deg. The minimum pulse is 45 deg with no phase margin. The orientation of the field with respect to the switch is shown in Figure 24.

These phase measurements explain the operation of the switch which may be visualized with the aid of Figure 24. As the bubble propagates under the conductor, the current pulse creates an attractive well under the leading edge of the conductor at A. The bubble will be trapped in this well and will be held for one period. To retard the bubble, the pulse has to be turned on before the bubble propagates out of the conductor at the trailing edge B. Therefore, the latest pulse timing is at 0 deg.

---

[23] T. T. Chen and J. L. Williams, "A Magnetic Bubble Retarding Switch," paper 3A-6 presented at the 23rd Magnetism and Magnetic Materials Conference, Minneapolis, Minn., 1977.
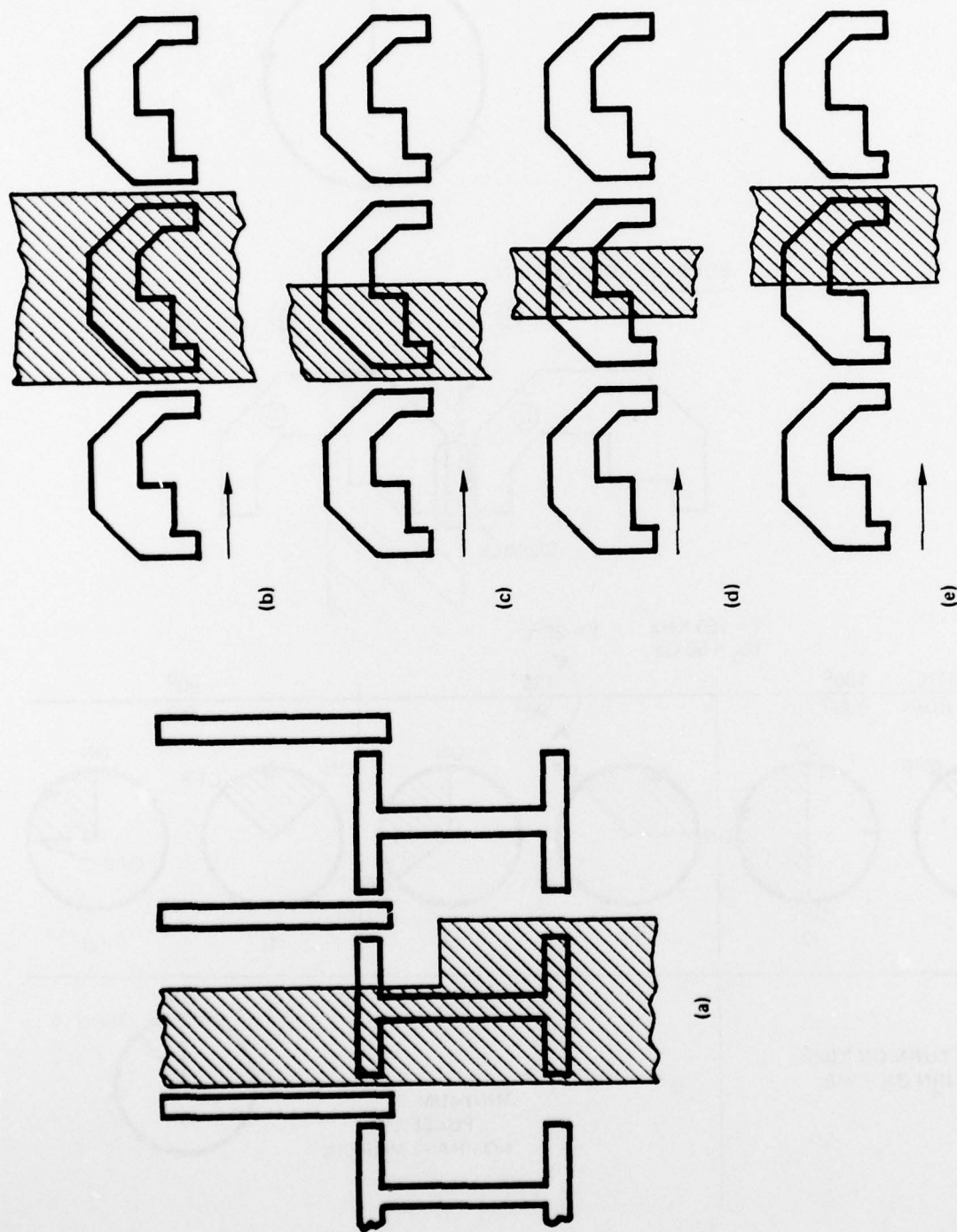
42
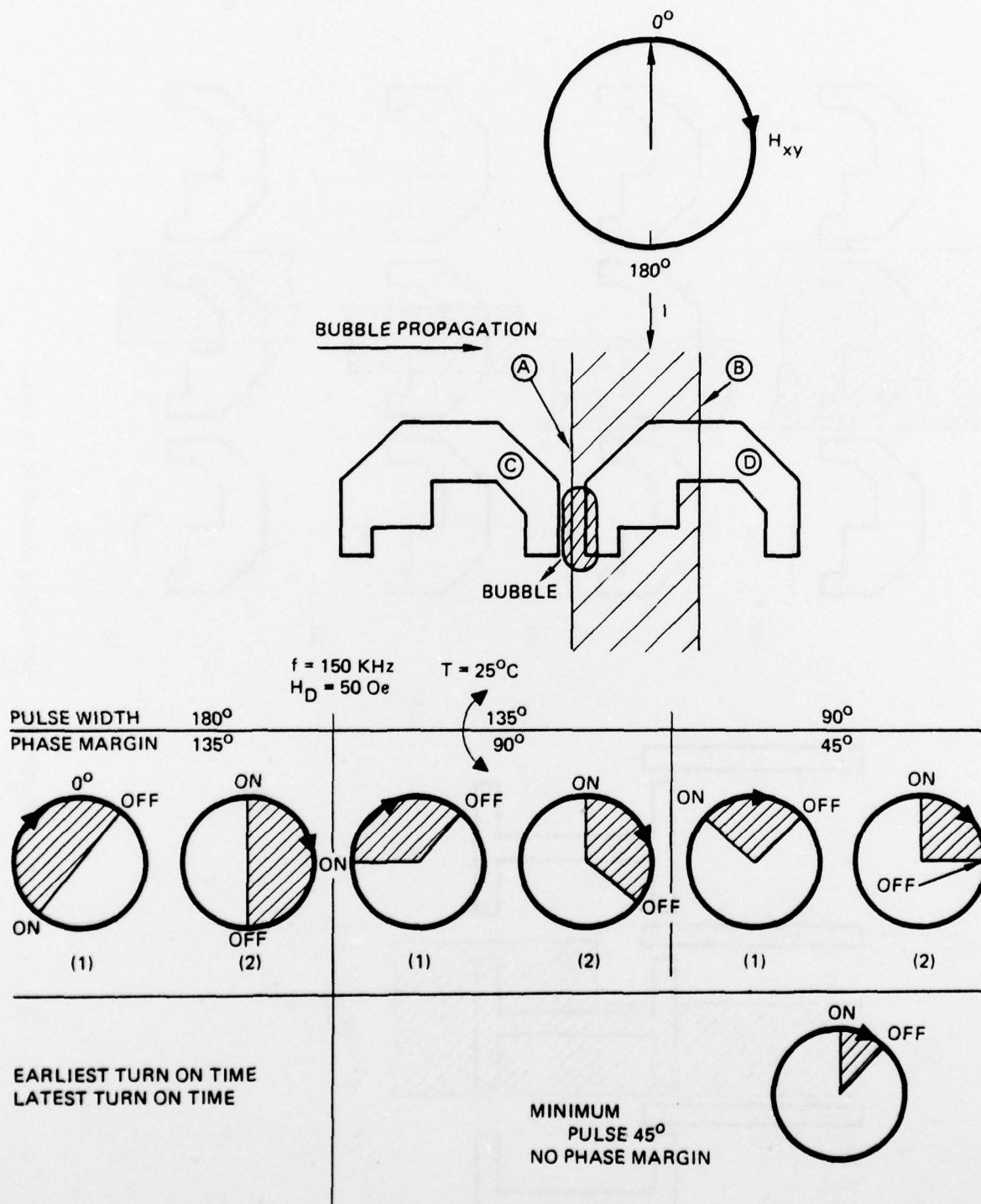
Figure 23. Retarding Switch of Designs

43

Figure 24. Phase Margin of the Retarding Switch

44

When the pulse is turned off, the in-plane field should create an attractive pole in the previous permalloy element to pull the bubble backward. This occurs at the 45 deg position where the pole generated at position C is close enough to prevent the bubble from moving forward to position D.

All the switch designs shown in Figure 23 work on the same principle and they all have good operating margins compared to the propagation element itself. Switch power and phase margin are the only parameters required to evaluate the various designs. To simplify the measurement and ease the comparison, data are taken by measuring the minimum switching current as a function of the pulse width. Figure 25 shows the result on a switch design where the conductor width equals to the full circuit period (Figure 24b). The solid line represents the minimum switch current required for a successful retardation by fixing the trailing edge of the current pulse at $\theta = 720$ deg and varying the leading edge of the pulse. The current has to be turned on before 630 deg or before the bubble propagates to the right leg of the half disk element giving a minimum pulse width of 90 deg. When the current pulse is turned on earlier than 360 deg, the minimum current drops accordingly, because the bubble travels less distance to the right end of the half disk element. When the current pulse is turned on before 540 deg, the current reaches a minimum of 55 mA which corresponds to a position where the bubble is under the wider half of the half disk element. As the pulsewidth extends beyond 270 deg, the bubble can be retarded for two cycles and the same current dependence pattern repeats.

The broken curve shows a similar measurement with the leading edge of the current pulse fixed at 145 deg and the trailing edge varied. Minimum turn-off time is at 270 deg for the pole generated in the element ahead of the switch to be close to the bubble held under the conductor. There is an unreliable region between 270 deg and 360 deg because the two poles in the switch element and the preceding element are competing with each other. The bubble may be attracted by either pole, split into two or even collapsed depending on the operating condition.

This pattern is repeated after one full cycle resulting in a 2-bit delay as in the previous case. Figure 26 shows a similar measurement for a switch design with conductor width equal to 1/3 of the circuit period. (Figuer 23d). The minimum switch current is reduced by more than 60 percent as expected but the minimum pulse width for such a low switch current is close to 360 deg. This is about two times the pulse width of the previous case because the conductor is placed at the center portion of the half disk element where the bubble does not spend much time during propagation. The large slope in the dotted curve found in Figure 26 is an indication the conductor current magnetizes the permalloy element outside of the conductor area pushing the bubble to the left end of the half disk element. By placing the bubble further to the left by increasing the current, the switch current can be turned off earlier.

Figure 27 shows the measurement on the switch design with conductor width equal to half of the circuit period and placed at the latter half of the half disk element. (Figure 23e). The minimum switch current rises to 32 mA because of the increased linewidth. The slope of the solid curve is less than that shown in Figure 25 because the bubble travelling distance is less. Little slope is found for the dotted curve which is due to the lack of overlap between the wide permalloy portion of the half disk element and the conductor.
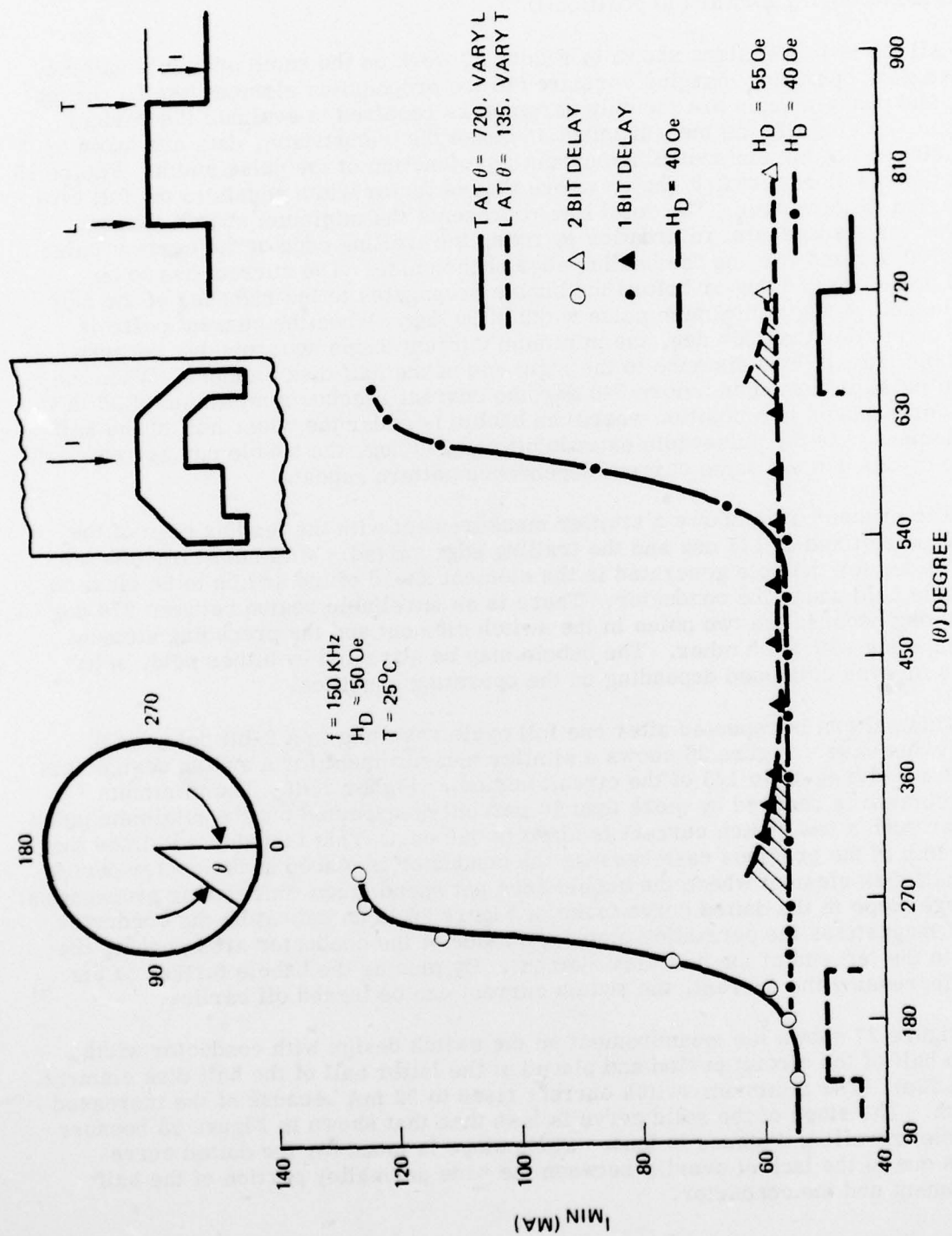
45

Figure 25. Phase and Current Margin of a Retarding Switch With Conductor Width Equal to Full Period
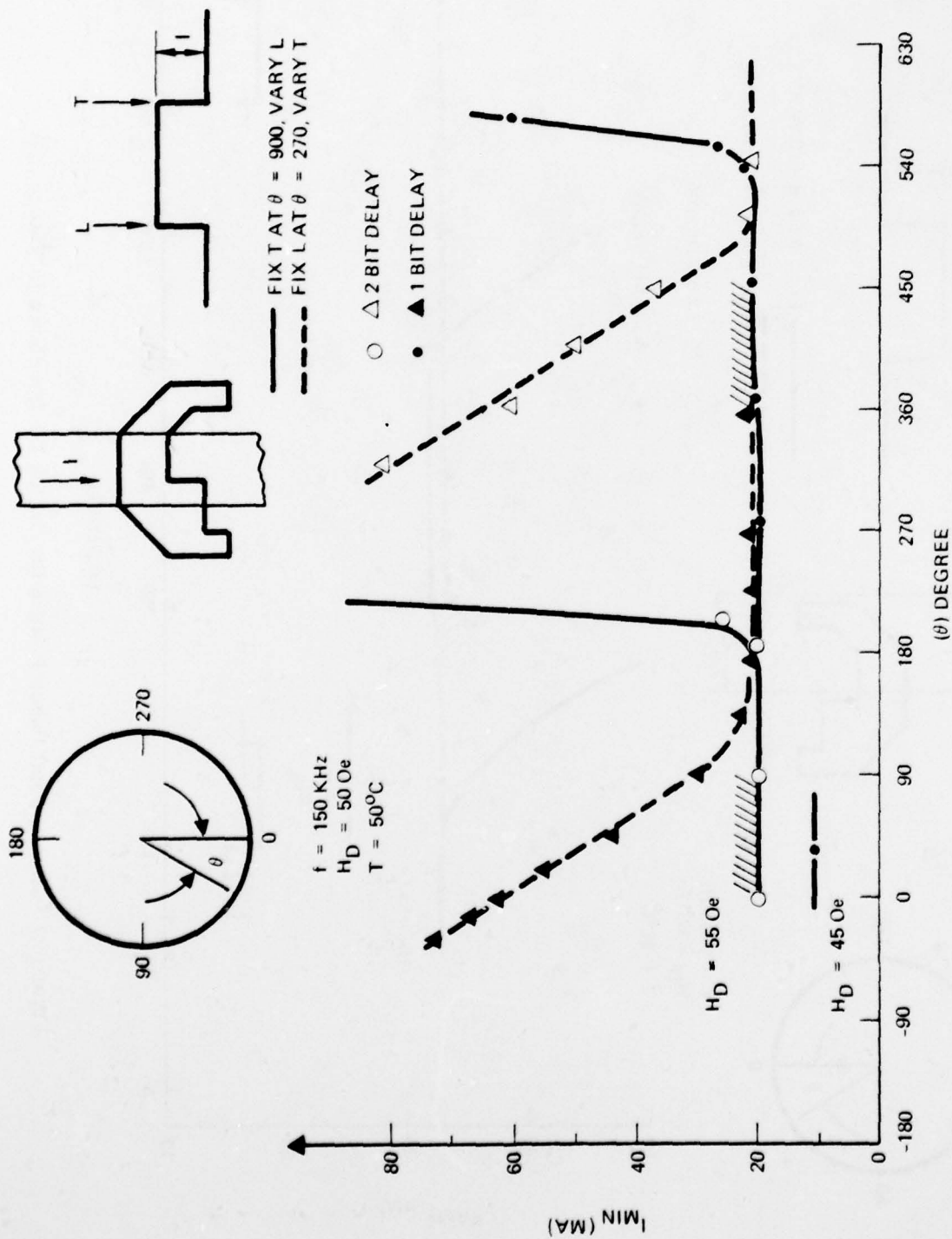
46

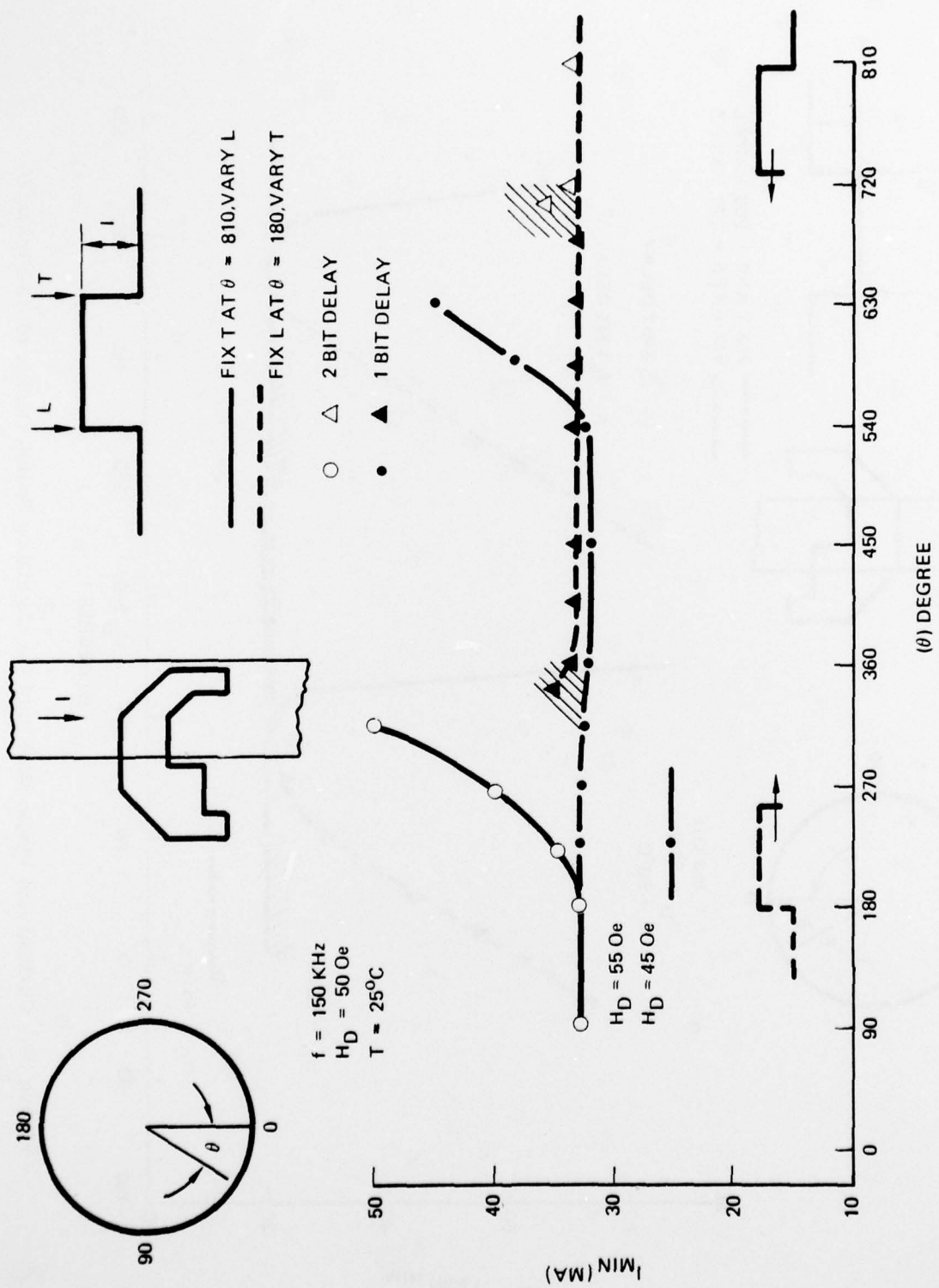Figure 26. Current and Phase Margin of the Retarding Switch Design (d) in Figure 23

47

Figure 27. Current and Phase Margin for Switch Design Shown in Figure 23e

From these observations it can be concluded that to optimize the retarding switch design, the conductor should be placed under the portion of the propagation element where the bubble will be held for the longest time. Also, it should be placed under the portion with the largest permalloy area such that the permalloy may enhance the potential well under the conductor. Thus the best design in Figure 23 is the one with conductor width equal to half of the period and placed at the first half of the circuit element (design C).

The measurement on this switch design is shown in Figure 28. The solid curve is almost flat and the broken curve shows some slope as in Figure 26. The minimum switching current is about 20 mA and the minimum pulsewidth at 26 mA is about 90 deg.

The minimum reliable pulse width at minimum pulse amplitude measured in Figures 25 to 28 are 55 mA-180 deg, 20 mA-360 deg, 32 mA-180 deg and 20 mA-135 deg respectively. If assuming the switch resistance ratio is inversely proportional to the conductor width, the power ratio between these switches is approximately $5 = 4 = 3 = 1$. Thus, the design in Figure 23c shows definite advantage in the switching power.

The operating margin of this switch design over the entire operating range was measured by the field interrupt technique using both bias and inplane field pulses. The results are shown in Figure 29. The minimum current varies by a factor of 2.3 over the entire operating range. This variation is caused by two factors. As the inplane field increases, it needs more retarding current to over-come the field gradient under the permalloy and when the bias field increases, the bubble size shrinks requiring higher switching current to transfer the bubble.

Further investigation of the switch operation was made by studying the potential well profile of the switch element. This was done by reducing the operating frequency to 12.5 kHz and using a short bias field pulse (4 μsec wide) to collapse the bubble while it was propagating under the permalloy element. This is the same technique that Singh and Hubble reported for T-bar element study (Ref 24). The collapse field so measured represents the local potential well variation under the permalloy element. A typical set of data is shown in Figure 30. The solid curve represents the bubble collapse field variation under the half disk element without switching current. It shows that the weakest position in the element is in the gap area. The deepest well (highest point in the curve) is in the first half of the element (at $\theta = 90$ deg) because of the large permalloy structure. This data is consistent with the strobiscopic observation of the bubble propagation under the permalloy circuit.

The dotted curve shows a similar measurement when the switch conductor is pulsed with 10 mA pulse. The pulse amplitude is low enough such that it will not impede the bubble propagation. The pulse width is wider than one cycle so that the current is always on when the bubble is under the switch element. The difference between the dotted curve and the solid curve represents the potential well difference induced by the current. In the region between 0 and 180 deg the effect is positive, and the largest difference is at 0 deg. This corresponds to an attractive pole located at the leading edge of the switch conductor. The largest negative effect occurs around 220 deg which corresponds to the trailing edge of the conductor located at the

---

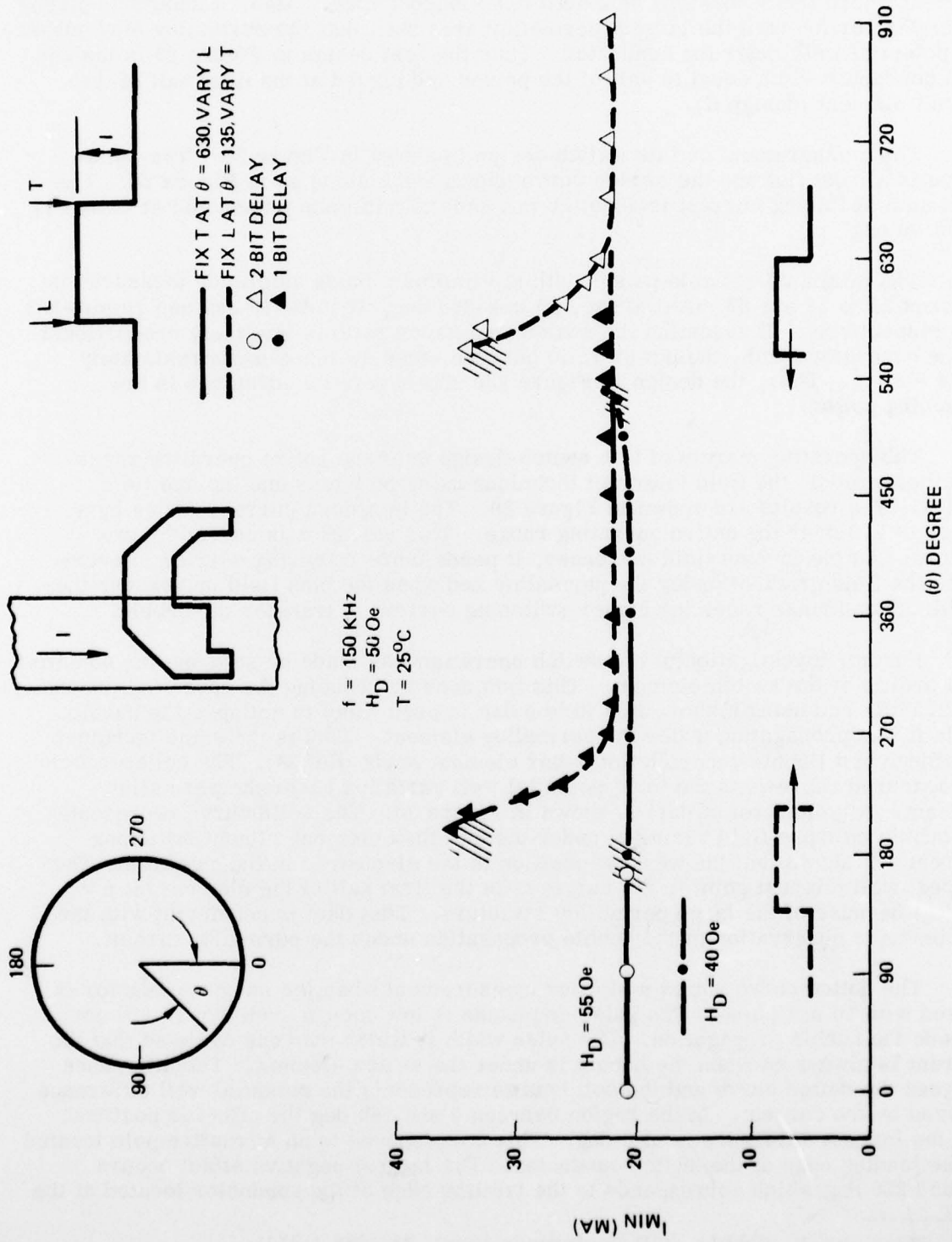[24] S. Singh and W. Hubble, AIP Conference Proc. 24, 638 (1974).

Figure 28. Current–Phase Margin of the Retarding Switch Shown in Figure 23c
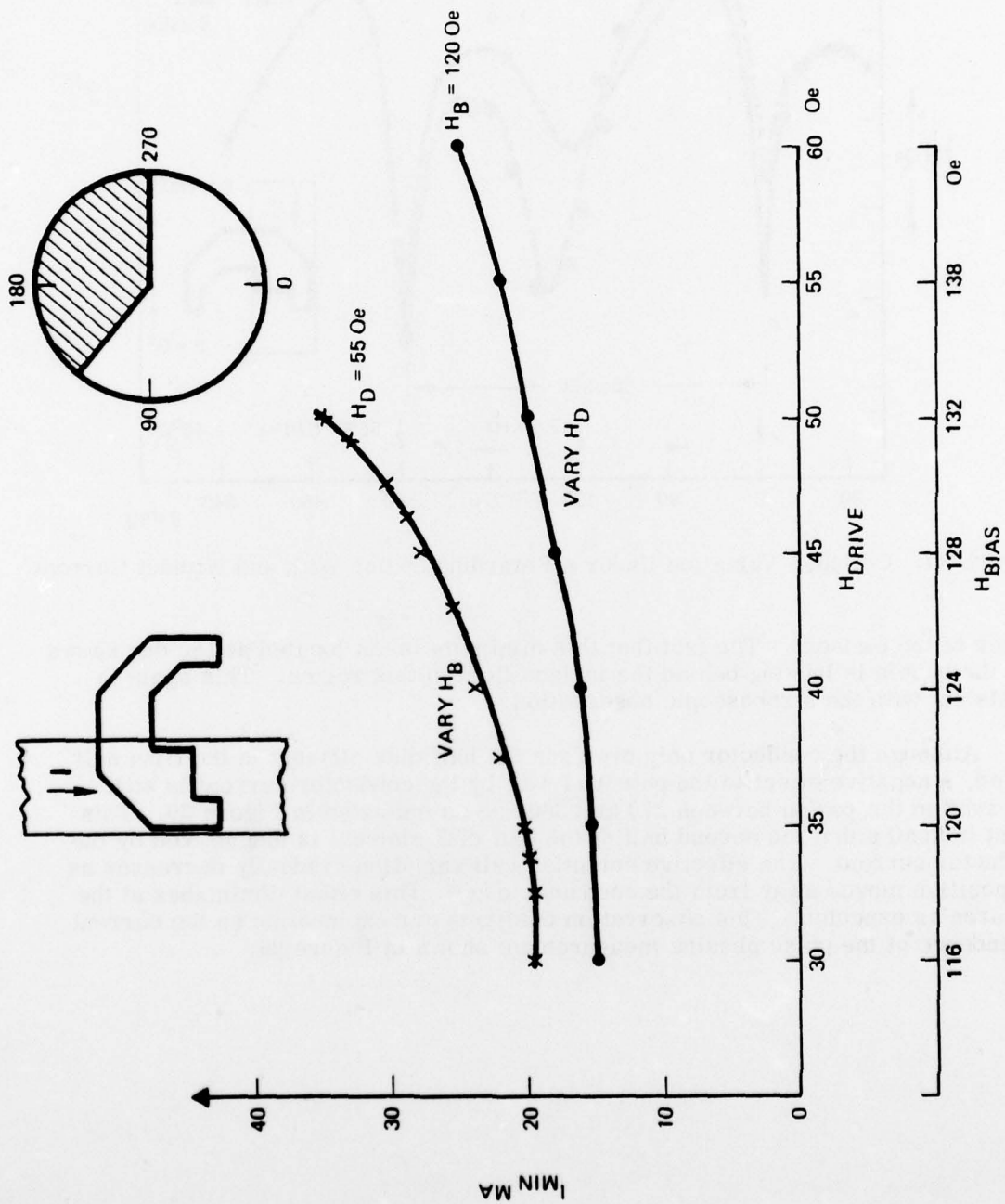
50

Figure 29. Minimum Switching Current Variation for Switch Design (c) in Figure 23
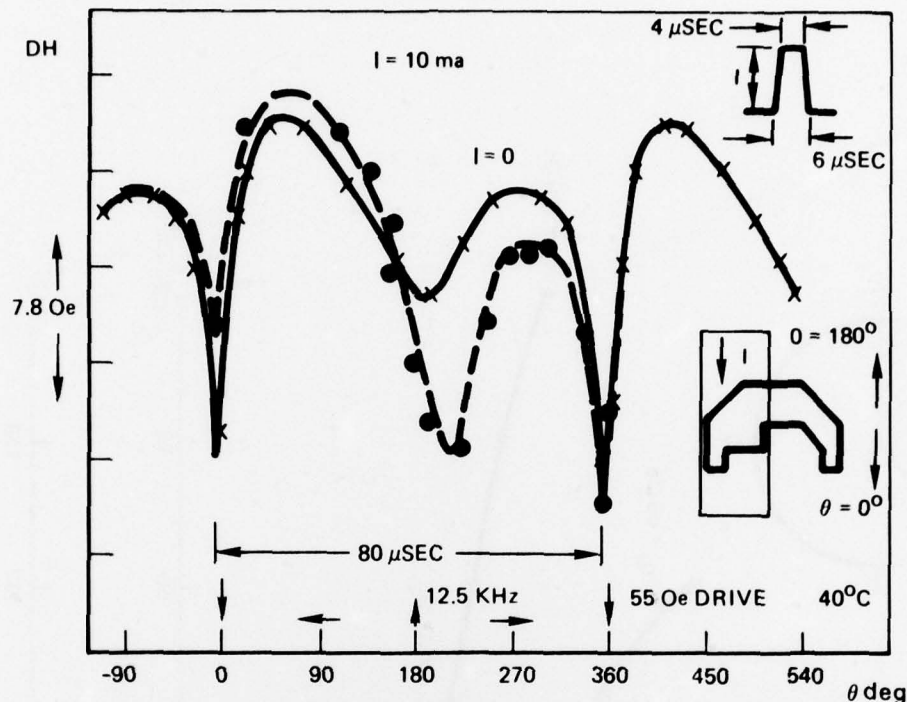
51

Figure 30. Collapse Variation Under a Retarding Switch With and Without Current

center of the element. The fact that this minimum is not located at 180 deg shows that the bubble is lagging behind the inplane field in this region. This again is consistent with the stroboscopic observation.

Although the conductor only overlaps the half disk element in the first half period, a negative effect to the potential well by the conductor current is still observed in the region between 270 and 360 deg as indicated in Figure 30. This effect indicates that the second half of the half disk element is magnetized by the conductor current. The effective potential well variation gradually decreases as the position moves away from the conductor edge. This effect diminishes at the gap area as expected. This observation confirms our explanation on the current dependence of the pulse phasing measurement shown in Figure 26.

REFERENCES

1. H. Uchishiba, H. Tominaga, T. Namikata, and S. Sakai, "Internal Bias Effect of Double Layer Epitaxial Garnet Films," IEEE Trans. Magn. MAG-9, 381 (1973).

2. H. Uchishiba, H. Tominaga, T. Obakata, and T. Manikata, "Growth and Properties of Stable Self Biasing Double Layer Epitaxial Garnet Films," IEEE Trans. Magn. MAG-10, 480 (1974).

3. H. Uchishiba, H. Tominaga, and K. Asama, "Temperature Stable Self-Biasing Bubbles in Double Layer Films," IEEE Trans. Magn. MAG-11, 1079 (1975).

4. P. J. Besser, T. T. Chen, D. M. Heinz, and T. Kobayashi, "High Density Magnetic Bubble Memory Techniques," Interim Report for 4 May 1976 to 4 November 1976, AFAL-TR-77-17, April 1977.

5. R. D. Henry, P. J. Besser, R. G. Warren and E. C. Whitcomb, "New Approaches to Hard Bubble Suppression," IEEE Trans. Magn. MAG-9, 514 (1973).

6. P. J. Besser, T. T. Chen, D. M. Heinz and T. Kobayashi, "High Density Magnetic Bubble Memory Techniques," Interim Report for November 4, 1976 to May 4, 1977, AFAL-TR-77-198, October 1977.

7. M. Nemiroff and H. Yue, "La:YIG Disks on GGG Substrates for Microwave Applications," IEEE Trans. Magn. MAG-13, 1238 (1977).

8. S. Geller, "Crystal Chemistry of the Garnets," Z. Krist. 125, 1 (1967).

9. S. L. Blank, J. W. Nielsen and W. A. Biolsi, "Preparation and Properties of Magnetic Garnet Films Containing Divalent and Tetravalent Ions," J. Electrochem. Soc. 123, 856 (1976).

10. M. Ketigian, A. B. Smith, and W. R. Bekebrede, "Magnetic Inhomogeneities in $(YSmCa)_3(FeGe)_5O_{12}$ and Their Elimination by Improved Growth Procedures," Mat. Res. Bull. 11, 773 (1976).

11. R. D. Shannon, "Revised Effective Ionic Radii and Systematic Studies of Interatomic Distances in Halides and Chalcogenides," Acta Cryst. A32, 751, (1976).

12. S. L. Blank, W. A. Biolsi and J. W. Nielsen, "The Effect of Melt Composition on the Curie Temperature and Flux Spin-Off from Lutetium Containing LPE Garnet Films," IEEE Trans. Magn. MAG-13, 1095 (1977).

13. S. Geller, H. J. Williams, G. P. Espinosa and R. C. Sherwood, "Importance of Intrasublattice Magnetic Interactions and of Substitutional Ion Type in the Behavior of Substituted Yttrium Iron Garnets," Bell System Tech. J. 43, 565 (1964).

14. R. C. Linares, "Growth of Refractory Oxide Single Crystals," J. Appl. Phys. 33, 1747 (1962).

15. R. D. Henry, P. J. Besser, R. G. Warren, and E. C. Whitcomb, "New Approaches to Hard Bubble Suppression," IEEE Trans. Magn. MAG-9, 514 (1973).

16. T. W. Liu, A. H. Bobeck, E. A. Nesbitt, R. C. Sherwood, and D. D. Bacon, "Thin-Film Surface Bias on Magnetic Bubble Materials," J. Appl. Phys. 42, 1360 (1971).

17. R. C. LeCraw, E. M. Gyorgy, and R. Wolfe, "Suppression of Hard Bubbles in LPE Garnet Films by Inert Atmosphere Annealing," Appl. Phys. Lett. 24, 533 (1974).

18. A. A. Thiele, "Theory of Cylindrical Magnetic Domains," Bell Syst. Tech. J. 48, 3287 (1969).

19 W. F. Druyvesteyn, D. L. A. Tjaden, and J. W. F. Dorleijn, "Calculation of the Stray Field of a Magnetic Bubble, with Application to Some Bubble Problems," Philips Res. Repts. 27, 7 (1972).

20. T. Kobayashi, D. M. Heinz, E. C. Whitcomb, P. J. Besser, and J. L. Archer, "Self-Biased Structures for Bubble Devices," 1977 Intermag Conf., paper 33-7, Los Angeles, June, 1977.

21. Y. Hidaka, K. Yoshimi, T. Hibiya, and M. Mikami, "Improved Propagation Margin in YIG Coated LPE Garnet Films for Bubble Devices," AIP Conf. Proc. 24, 633 (1974).

22. H. Callen and R. M. Josephs, "Dynamics of Magnetic Bubble Domains with an Application of Wall Mobilities," J. Appl. Phys. 42, 1977 (1971).

23. T. T. Chen and J. L. Williams, "A Magnetic Bubble Retarding Switch," paper 3A-6 presented at the 23rd Magnetism and Magnetic Materials Conference, Minneapolis, Minn., 1977.

24. S. Singh and W. Hubble, AIP Conference Proc. 24, 638 (1974).